Indian Geotechnical Journal, 40(4), 2010, 207-242

Grundbaumechanique/Geomechanics Revisited
A New Paradigm for Geotechnical Engineering[1]

Madhira R Madhav[2]

Key words

Consolidation, non-linear theory, consolidation by PVDs, bearing capacity, leaning instability, uncoupled moduli, strain induced non-homogeneity

Abstract: The paper revisits the basic tenets of Geotechnical Engineering as propounded by its founders in the early years such as (i) rigid plasticity, (ii) leaning instability, (iii) thin versus thick layer response, (iv) inelastic response, (v) stress or strain induced non-homogeneity, etc. Conventional approaches for the estimation of the ultimate capacities of both shallow and deep foundations use limit equilibrium methods and are based on only the strength parameters apart from the geometry of the foundation element. Ground/soil being a much more complex material than metals from which the original theories have been developed, requires the consideration of stiffness or compressibility as well as the strength parameters for the estimation of ultimate loads. The results for the bearing capacity of shallow foundations, the ultimate axial capacity of piles and for leaning instability of tall structures show dependence on the stiffness of the ground. The conventional one-dimensional consolidation theory developed by Terzaghi is based on linear void ratio-effective stress relationship and for thin layers only. A theory of non-linear one-dimensional consolidation of a thick clay deposit considering linear void ratio-log effective stress relationship that incorporates the variation of initial in-situ effective stress with depth indicates that the conventional thin layer theory underestimates the degree of consolidation and overestimates the degree of dissipation of excess pore pressures. The degree of settlement and degree of dissipation of pore pressures are sensitive to the magnitude of applied load unlike in the conventional thin layer theory. The effects of the non-linear theory for radial flow in to vertical drains has similar effects on degree of settlement, degree of dissipation of excess pore pressure and variation of excess pore pressures with respect to time, radial distance and depth. An interesting outcome is the induced vertical flow in a radial flow problem. Response of ground is inelastic and moduli of deformation in compression and on unloading are significantly different from each other. The moment influence coefficient considering inelastic response of ground (as part of the foundation gets unloaded due to moment loading), for different rectangular, circular and annular foundations is a function of the relative modulus, R_k, the ratio of subgrade moduli in unloading to that in compression. Estimation of distribution of displacements and stresses in the soil mass resulting from the loads applied at or below the surface is one of the basic challenges in foundation engineering/soil-foundation interaction studies. Estimating the parameters E and G from by the direct shear test, a new simple two parameter model based on uncoupled deformation, E, and shear, G, moduli, is proposed for analysing stresses and displacements under a rigid or uniformly loaded circular footing on a finite layer. The elastic continuum and Vlasov models are obtained as particular cases of the proposed solution. An analysis that incorporates strain dependency of deformation modulus of soils leads to strain induced non-homogeneity for the ground. Results obtained highlight the importance of considering strain induced non-homogeneity on settlement of foundations.

There is Life in the Ground:
it goes into the seed and it also,
when stirred up, goes into the
man who stirs it.
C. D. Warner

Introduction

Soil is unique amongst all Civil Engineering materials. Metals such as steel, iron, aluminum, copper, etc., gave rise to the field of Mechanics of Solids. Concrete which came into use much later fitted somewhat in to the same framework of mechanics. Water amongst the fluids gave birth to the principles of fluid mechanics. Study of soil as an engineering material was practically unheard of except for Coulomb in 18th (shear strength) century and Reynolds in the 19th century (dilatancy). Even in the early twentieth century, the ideas related to plasticity have been borrowed from an agricultural scientist, Atterberg. Though Collins in 1846 measured the profile of a failure surface as a cycloid, it was left to Petterson in 1919 to propose the method of slices for the analysis of stability of slopes. Terzaghi rightfully is credited as the father of Soil Mechanics, for he in 1925 had put together scientific principles, especially, the principle of effective stress, to understand or explain the behaviour of soils.

Historically therefore it is but natural that several principles of mechanics derived and applied to metals and several solid-like materials, are extended to study the behaviour of soils. Thus we have the concepts of linear theory of elasticity, isotropy, homogeneity, coupling between modulus of elasticity, E, and shear modulus, G, {= E/(1+2ν)}, time independent

1 IGS Ferroco Terzaghi Oration 2010 delivered on 4 October 2010 at Bangalore, India

2 Emeritus Professor, JNT University Hyderabad, India, Email: madhavmr@gmail.com

deformations except for creep, materials without memory, uncoupled strains or deformations (volumetric strains only due to normal stresses and not due to shear stresses), stress path or strain independent modulus, rigid plasticity (negligible or little deformation or strain before failure), Tresca and von Mises failure criteria which do not account for the angle of shear resistance or friction angle, size independent response of materials (i.e. gravity has no influence), etc.

Stress – Strain Relationships

The stress – strain relationships of various engineering materials are shown in Figures 1(a) and (b) in linear and log-log scales. Soils are so weak and highly deformable that their stress – strain curves for are not visible when plotted on a linear scale in comparison with those of steel and concrete but become discernable if plotted on log-log scale. The ultimate strength and stiffness of steel are respectively 415 MPa and 210 GPa while those of soils possibly range between 10 (soft clay) to 400 kPa (dense sand) and 0.5 to 10 MPa respectively. Thus these plots contrast the significantly large differences in the strength and stiffness of soils in comparison with those of steel and concrete.

Bearing Capacity of Shallow Foundations

Prandtl's theory originally developed for metals with compressive and tensile strengths of nearly the same magnitude, i.e. with friction angle equal to zero, is the starting point for the estimation of bearing capacity of shallow foundations. Terzaghi (1943) modified the same and proposed his famous theory for strip footing resting on cohesive-frictional soils (Figure 2) an active wedge defined by the angle of shearing resistance, ϕ, and the passive wedges defined by the angle, $(\phi/4-\pi/2)$ both with respect to the horizontal. Prandtl's solution modified for c-ϕ soils (c being the cohesion) with the active wedge defined by $(\phi/4+\pi/2)$ instead is adopted as the basis for the estimation of ultimate bearing capacity, q_{ult}, of foundations, as

$$q_{ult} = cN_c s_c + qN_q + 0.5\gamma BN_\gamma s_\gamma \qquad (1)$$

where N_c, N_q and N_γ are the bearing capacity factors

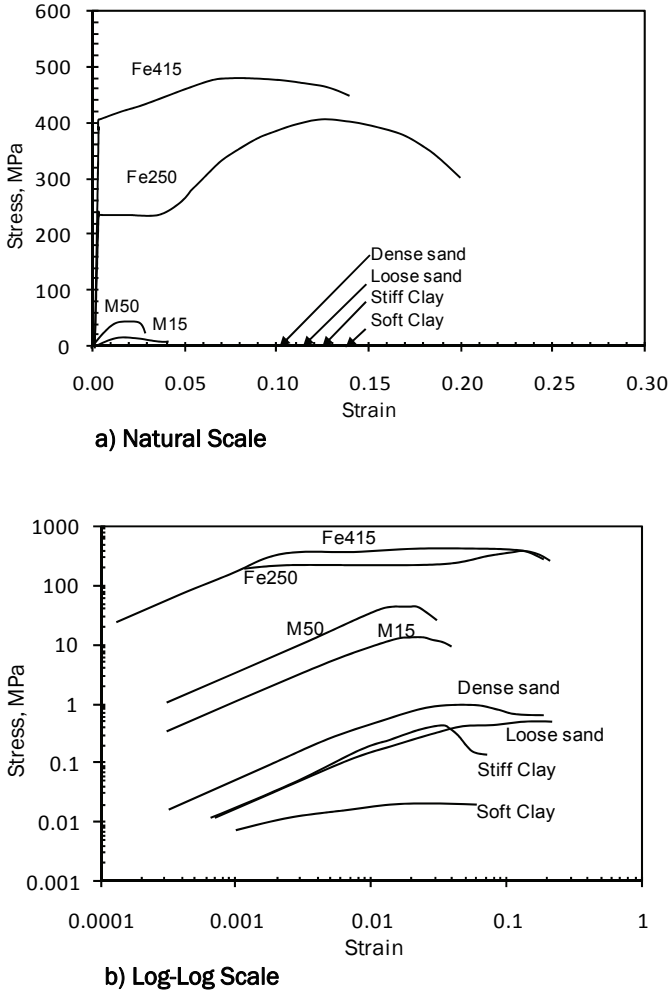

Fig. 1 Stress-Strain Variations for Various Engineering Materials

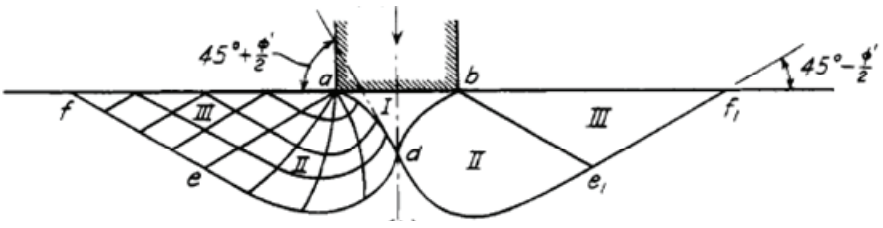

Fig. 2 General Shear Failure in c - ϕ Soils (Terzaghi, 1943)

while s_c, s_q and s_γ – the shape factors. It was soon realized that real soils do not fail in 'general shear failure' and a new failure mode, termed 'local shear failure' was identified as a possible alternative. The ultimate bearing capacity of footings based on local shear failure is estimated empirically (Terzaghi and Peck 1967) with the same equation (Eq. 1) as above but with both the strength parameters, c and tan ϕ reduced to 2/3rd the corresponding values. Vesic (1973) extended this concept and identified a third failure mode, 'punching shear failure' occurring in loose soils at shallow depths and at depth in case of dense soils. Figure 3 (Lambe and Whitman 1969) classifies the three failure modes as dependent on both the relative density of granular soils and the relative depth, D/B, of the footing.

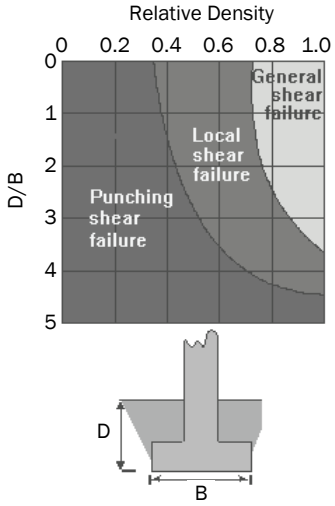

Fig. 3 Modes of Foundation Failure in Sand (after Vesic, 1973)

Effect of Stiffness of Ground – Cavity Expansion Theory

Gibson and Anderson (1961) present a plasticity solution for the limit pressure, p_l, for the expansion of a cylindrical cavity in an undrained soft soil. Menard (1957d) obtained the limit pressure for the cylindrical cavity for cohesive soils in the form of an expression very similar to that for the bearing capacity of a footing as

$$p_l = \sigma_h + c_u N_c^* \qquad (2)$$

where $N_c^* = 1 + \ln(G/c_u)$, G and c_u are respectively the shear modulus and undrained strength of soft soil and σ_h is the total horizontal stress in the ground. The factor, N_c^*, which for the first time incorporates the relative stiffness of the ground with respect to the strength, increases (Figure 4) with increase in relative stiffness

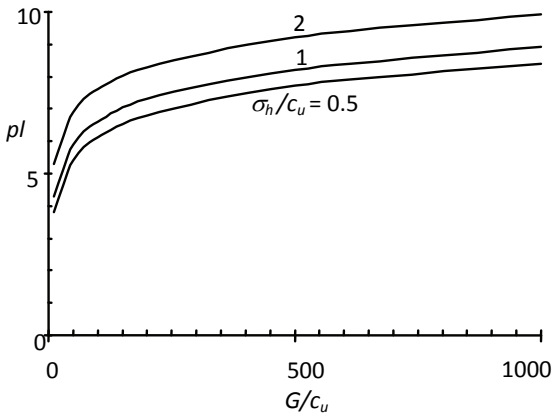

Fig. 4 Variation of Limit Pressure with Shear Stiffness and Total Horizontal Stress

ratio, G/c_u. Thus the limit pressure is dependent on the shear stiffness apart from the undrained strength of the soil. Similar expressions have been derived by Vesic (1972) for estimating the limit pressure for the expansion of cylindrical cavity in a soil possessing both cohesion and friction as

$$p_l = c' F_c' + \sigma_h F_q' \qquad (3)$$

where $F_q' = (1+\sin\phi')(I_{rr}' \sec\phi')^{\sin\phi'/(1+\sin\phi')}$,

$F_c' = (F_q' - 1)\cot\phi'$, and

$I_{rr}' = (G/c' + \sigma_h' \tan\phi')/\{1 + (G/c' + \sigma_h \tan\phi')\Delta V_p \sec\phi'\}$,

F_c' and F_q' are the cavity expansion factors for cohesion and soil stress respectively, I_{rr}' - a rigidity factor.

Figure 5 (Madhav and Padmavathi 2008) depicts the variation of ratio, R_q (p_l of compressible

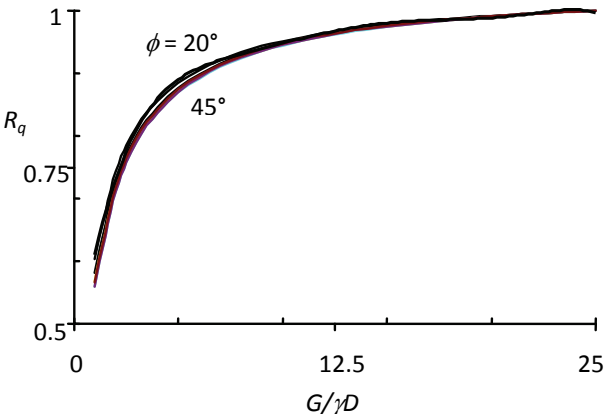

Fig. 5 Variation of R_q with $G/\gamma D$ and ϕ for dVp = 0.3 and $c/\gamma D$ = 0.5

ground/p_l of incompressible ground, i.e. G→∞), of limiting pressure of the soil with respect to the limiting pressure of the soil with infinite rigidity (i.e. *G* tending to infinity), with the normalised stiffness, $G/\gamma D$, and the angle of shearing resistance for drained conditions, ϕ', where *D* is depth of the footing from ground level. R_q increases with increase in stiffness for low values of $G/\gamma D$ for different angles of shear resistance but is nearly independent (Figure 5) of the angle of shearing resistance for given stiffness, volumetric strain, ΔV_p = 0.3 and $c/\gamma D$ = 0.5. The ratio, R_q, of limiting pressures, increases with increase in normalised stiffness of the soil (Figure 6) for volumetric strain of 0.3% and ϕ' = 30°. The effect of $c/\gamma D$ on R_q is remarkable for the normalised stiffness less than 15. Figure 7 shows the variation of R_q with rigidity factor, I_{rr}, and angle of shear resistance, ϕ', for $c/\gamma D$ = 0.5 and volumetric strain = 0.3%. The values of R_q increase with I_{rr} for any given ϕ' value and with ϕ' for given I_{rr}.

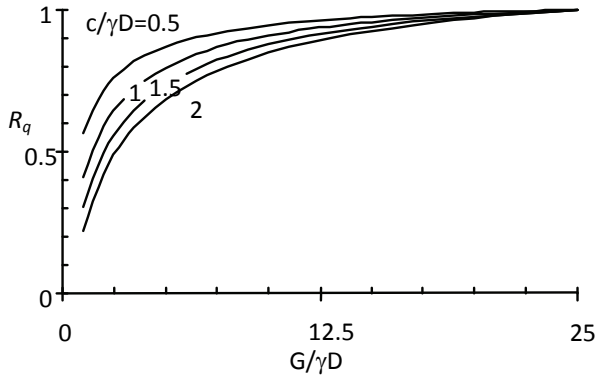

Fig. 6 Variation of R_q with $G/\gamma D$ and $c/\gamma D$ for dVp=0.3 and ϕ=30°

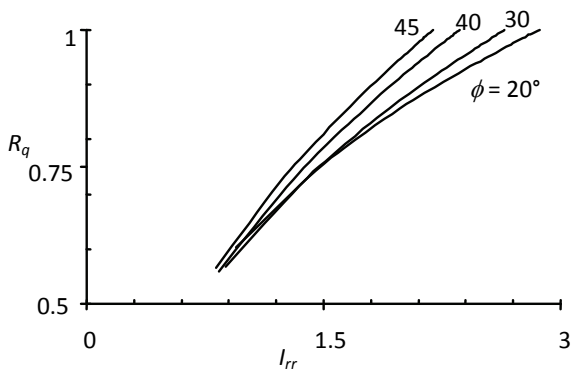

Fig. 7 Variation of R_q with I_{rr} and ϕ for dVp = 0.3 and $c/\gamma D$ = 0.5

Bearing Capacity Inclusive of Stiffness or Compressibility of Ground

Vesic (1973) proposed a general expression accounting for compressibility of the ground/soil as

$$q_u = c'N_cF_{cs}F_{cd}F_{cc} + qN_qF_{qs}F_{qd}F_{qc} + 0.5\gamma BF_{\gamma s}F_{\gamma d}F_{\gamma c} \quad (4)$$

where F_{cc}, F_{qc}, $F_{\gamma c}$ are the compressibility factors, F_{cs}, F_{qs}, $F_{\gamma s}$ – the shape factors and F_{cd}, F_{qd}, $F_{\gamma d}$- the depth factors. These factors were derived based on expansion of cavity. F_{cc}, F_{qc}, $F_{\gamma c}$ are obtained in terms of rigidity index, I_r, of the soil at a depth approximately, $B/2$, below the bottom of the foundation, as I_r = G/(c'+q'tanϕ') and q' = $\gamma(D + B/2) = q + \gamma B/2$. The critical rigidity index, $I_{r(cr)}$, for rigid plastic condition is

$$I_{r(cr)} = 0.5\left\{\exp\left[\left(3.3 - 0.45\frac{B}{L}\right)\cot\left(45 - \phi'/2\right)\right]\right\} \quad (5)$$

The compressibility factors, F_{cc}, F_{qc}, $F_{\gamma c}$, are given as

For $I_r < I_{r(cr)}$;

$$F_{\gamma c} = F_{qc} = \exp\left\{\left[\left(-4.4 + 0.6\frac{B}{L}\right)\tan\phi' + \left[\frac{(3.07\sin\phi')(\log 2I_r)}{1+\sin\phi'}\right]\right]\right\} \quad (6)$$

For ϕ = 0° F_{cc} = 0.32 + 0.12 (B/L) + 0.6 log(I_r) and for ϕ' > 0° $F_{cc} = F_{qc} - ((1-F_{qc})/N_q \tan\phi')$. Eq (4) is normalized as

$$q_u/\gamma B = (c'/\gamma B)\, N_cF_{cs}F_{cd}F_{cc} + (D/B)N_qF_{qs}F_{qd}F_{qc} + 0.5N_\gamma F_{\gamma s}F_{\gamma d}F_{\gamma c} \quad (7)$$

For $I_r \geq I_{r(cr)}$; $F_{cc} = F_{qc} = F_{\gamma c} = 1$, and correspond to rigid plastic behaviour (general shear failure). The

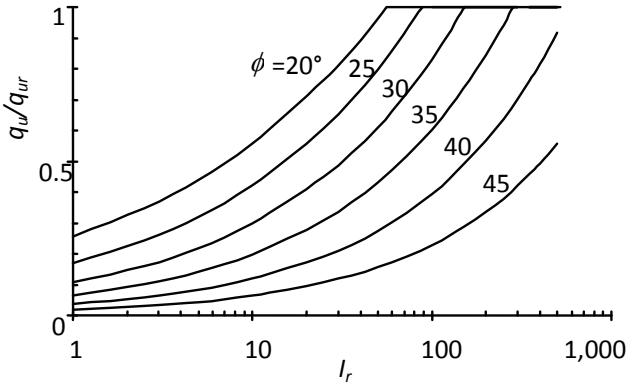

Fig. 8 Variation of Ultimate Bearing Capacity Ratio q_u/q_{ur} with I_r and ϕ for B/L=0, $c'/\gamma B$=0, D/B = 1

bearing capacity ratio, q_u/q_{ur}, increases with increase in rigidity index, I_r, for given ϕ, B/L = 0, $c'/\gamma B$ = 0, D/B = 1 (Figure 8). The limiting value of I_r beyond which the bearing capacity ratio remains constant at one, is 90 for ϕ=25° and 300 for ϕ=35°.

General shear failure is indicated for I_r values greater than the limiting values given above. Figures 9, 10 and 11 show the variations in the ratio, q_u/q_{ur}, with I_r and $c'/\gamma B$ for B/L = 0, D/B = 1 and ϕ = 20°, 30° and 45° respectively. The ratio, q_u/q_{ur}, is very small, of the order of 0.1 or less for very compressible soils and increases gradually with I_r till the ratio attains the value of 1.0 corresponding to general shear failure at the limiting value of I_{rr} given above. The limiting value of I_r is independent of $c'/\gamma B$ for a given value of ϕ. The ratio, q_u/q_{ur}, is nearly independent of $c'/\gamma B$ for ϕ = 45°. Similarly the ratio, q_u/q_{ur}, is not very sensitive (Figure 12) to the ratio D/B varying from 0.5 to 3 especially at higher I_r value.

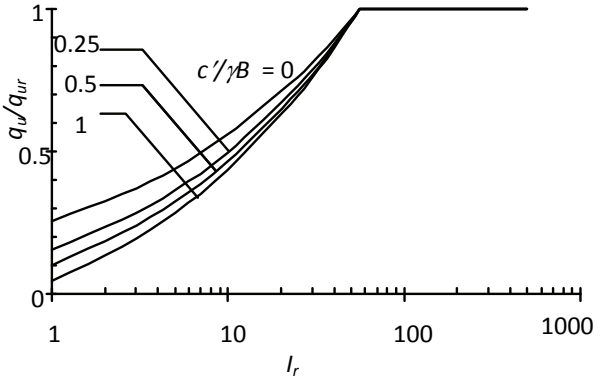

Fig. 9 Variation of q_u/q_{ur} with I_r and $c'/\gamma B$ for B/L = 0, ϕ = 20°, D/B = 1

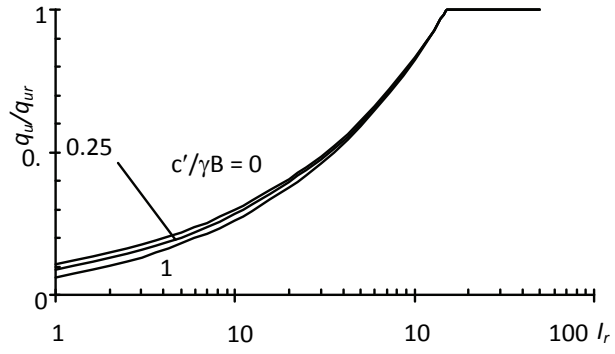

Fig. 10 Variation of q_u/q_{ur} with I_r and $c'/\gamma B$ for B/L = 0, ϕ = 30°, D/B = 1

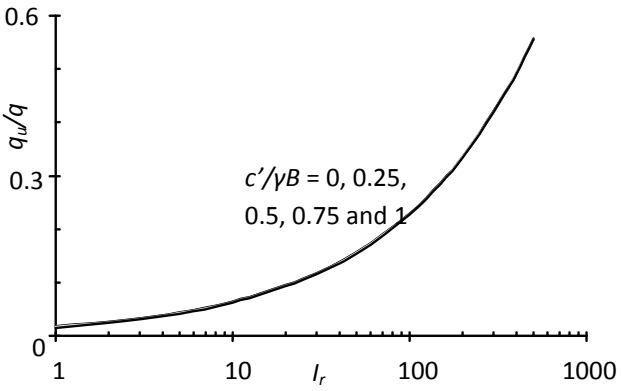

Fig. 11 Variation of q_u/q_{ur}, with I_r and $c'/\gamma B$ for B/L = 0, ϕ = 45° and D/B = 1

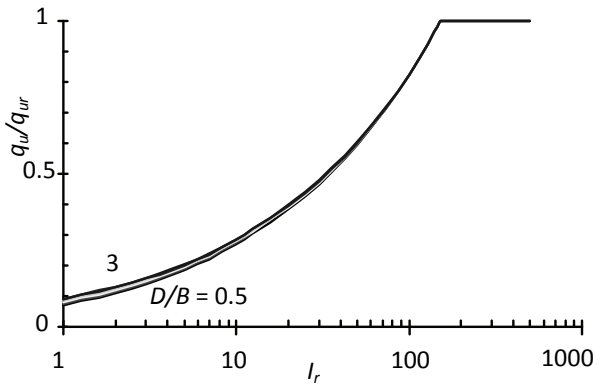

Fig. 12 Variation of q_u/q_{ur}, with I_r and D/B for B/L = 0, ϕ = 30 and $c'/\gamma B$ = 0.5

The limiting value of I_r increases with increase in angle of shearing resistance, ϕ, as shown in Figure 13 for B/L = 1, D/B = 1, $c'/\gamma B$ = 0.5. The limiting value of I_r is about 40 for ϕ of 25° and increases to 500 for ϕ equal to 45°. The ratio, q_u/q_{ur}, is very sensitive to ϕ decreasing from about 0.52 for ϕ = 25° and to about 0.12 for ϕ = 45° for I_r = 10. This figure brings out the significant effect of stiffness of the granular soils on the ultimate bearing capacity.

The variations of the bearing capacity ratio, q_u/q_{ur}, with I_r, for strip, square and rectangular footings are shown in Figure 14. The limiting value of I_r deceases from about 150 for B/L = 0 (strip) to 70 for B/L = 1 (square), for D/B = 1, ϕ = 30°, $c'/\gamma B$ = 0.5. Similar variation of q_u/q_{ur} with I_r for different B/L ratios is shown in Figure 15 for ϕ = 45°, D/B = 1 and $c'/\gamma B$ = 0.5. While the trend in the variation of q_u/q_{ur} with I_r for ϕ = 45° is similar to that $\phi = 30°$, the curves do not indicate any limiting values of I_r in this case. The difference in the values of q_u/q_{ur} for B/L increasing from 0 (strip) to 1 (square) is 0.45 for I_r=500, and less than 0.05 for I_r<10.

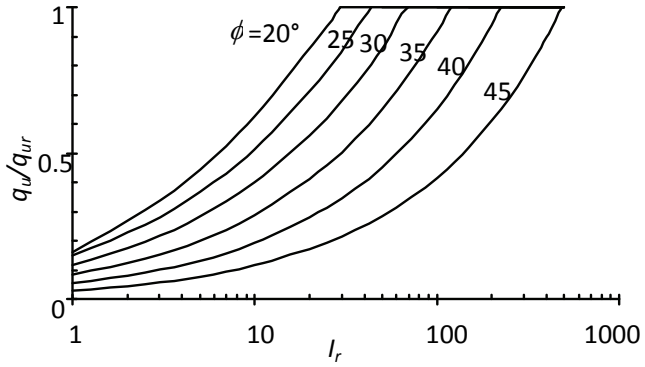

Fig. 13 Variation of Ultimate Bearing Capacity Ratio, q_u/q_{ur}, with I_r and ϕ for B/L = 1, D/B = 1, and $c'/\gamma B$ = 0.5

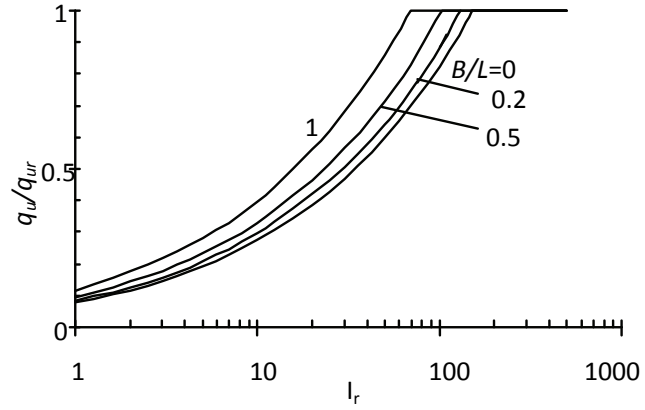

Fig. 14 Variation of q_u/q_{ur} with I_r and B/L for D/B = 1, ϕ = 30°, $c'/\gamma B$ = 0

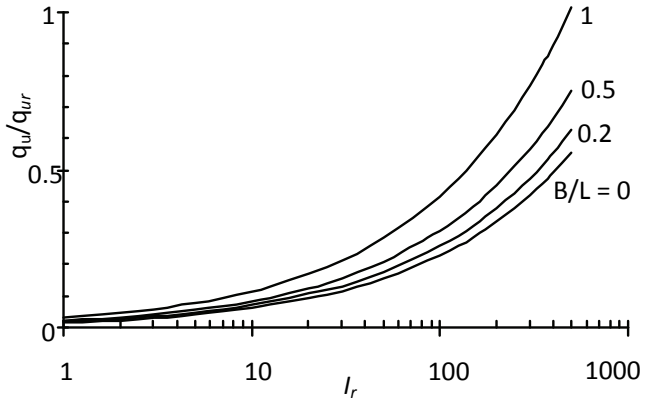

Fig. 15 Variation of q_u/q_{ur} with I_r and B/L for D/B = 1, ϕ = 45° and $c'/\gamma B$ = 0.5

Effect of Stiffness or Compressibility on Ultimate Point Resistance

The proposed equation (Vesic 1977) for point or end bearing resistance, q_{pu}, of the pile based on cavity expansion theory is

$$q_{pu} = c'N_c^* + \sigma_{av}'N_\sigma^* \quad (8)$$

where $\sigma_{av}' = ((1+2K_0)/3)q'$, $N_\sigma^* = f(I_{rr})$, $I_{rr} = I_r/(1+I_r.\varepsilon)$. For undrained condition ($\phi = 0^\circ$) $N_c^* = (4/3)(\ln I_{rr} + 1) + \pi/2 + 1$, N_c^*, N_σ^* are the bearing capacity factors for cohesion and stress respectively, σ_{av}' = mean effective normal overburden stress at the level of pile base, K_0 = earth pressure coefficient at rest = 1- sin ϕ', I_{rr} = reduced rigidity index for the soil, ε = average volumetric strain in the plastic zone below the pile point.

Figure 16 depicts the variation of the ratio, q_{pu}/q_{pur}, of the ultimate point resistance for compressible ground to the ultimate bearing resistance for the pile on incompressible ground, (the ratio of ultimate capacity of the pile considering compressibility to that on very stiff foundation) with I_r for given ϕ, D/B = 10 and $c'/\gamma B$ = 0.5. q_{pu}/q_{pur} decreases from about 0.25 to 0.1 for ϕ increasing from 20 to 50° for I_r = 10, D/B = 10 and $c'/\gamma B$ = 0.5. Thus the effect of compressibility of the ground is more for soils with higher friction angles. q_{pu}/q_{pur} values for all values of ϕ converge at higher values of I_r. The variation of q_{pu}/q_{pur} with I_r is independent of D/B (Figure 17) in the range 10 to 100 for ϕ = 30° and $c'/\gamma B$ = 0.5. $c'/\gamma B$ has no effect (Figure 18) on the variation of q_{pu}/q_{pur} with I_r for ϕ = 30° and D/B =10. Figure 19 shows the variation in q_{pu}/q_{pur} with relative stiffness or rigidity factor, I_r, and volumetric strain, ε, for $c'/\gamma B$ = 0.5, ϕ =30° and D/B =10. q_{pu}/q_{pur} increases with increase in I_r for any

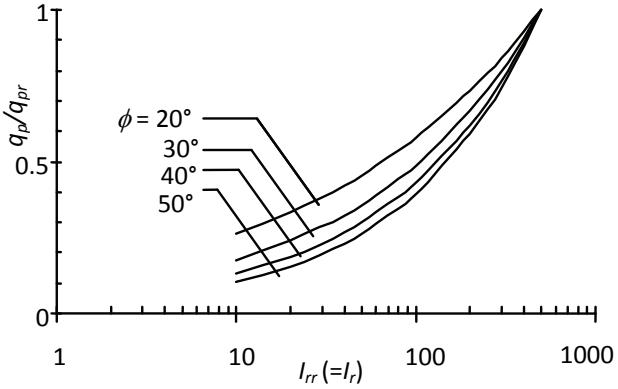

Fig. 16 Variation of Ultimate Point Bearing Capacity Ratio q_{pu}/q_{pur} with I_r and ϕ for D/B = 10, $c'/\gamma B$ = 0.5

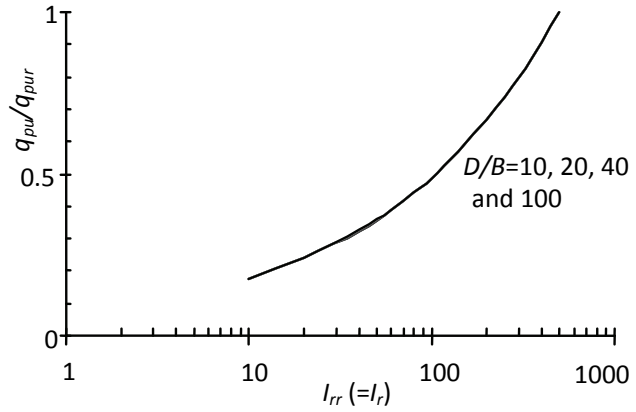

Fig. 17 Variation of Ultimate Point Capacity Ratio q_{pu}/q_{pur} with I_r and D/B for $\phi = 30°$, $c'/\gamma B = 0.5$

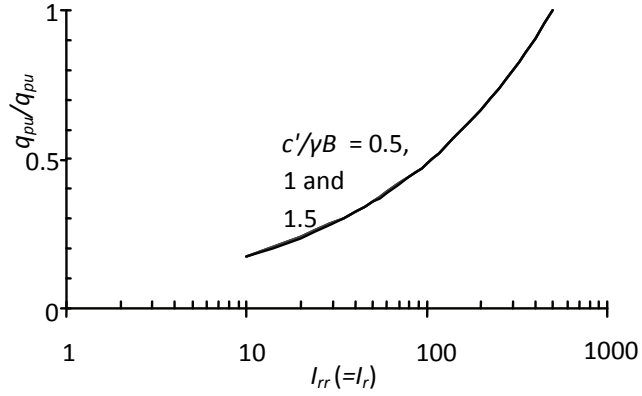

Fig. 18 Variation of Ultimate Point Capacity Ratio q_{pu}/q_{pur} with I_r and $c'/\gamma B$ for $\phi = 30°$, $D/B = 10$

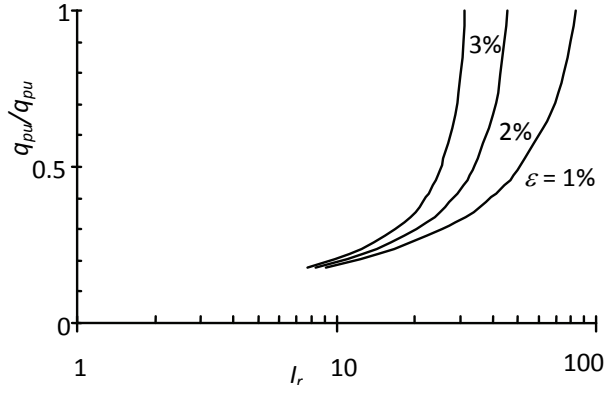

Fig. 19 Variation of Ultimate Point Bearing Capacity Ratio q_{pu}/q_{pur} with I_r and ε for $c'/\gamma B = 0.5$, $\phi = 30°$, D/B = 10

specified volumetric strain. The value of rigidity factor decreases with increase in volumetric strain. The limiting rigidity factor is 25 for ε = 3% and increases to 80 for ε = 1%.

Effect of Height of Structure and Leaning Instability

Another of Terzaghi's simplification has been the neglect of the influence of the effect of the structure on its stability. While the stability of structures founded on or in the ground should have been considered only the stability or the bearing capacity of foundations resting on or in the ground was considered as described above. Recent works of Hambly (1985 and 1990), Cheney et al. (1991), Lancelotta (1993) and Potts (2003) quantify the effect of the height of the structure on its stability somewhat akin to that of buckling of long columns. Incidentally, the buckling of long slender columns is controlled by the flexural stiffness of the structure and not the strength of the material.

Figure 20 depicts a tall structure of weight, W, with its centre of gravity at height, h, resting on homogeneous ground characterized by the coefficient of subgrade reaction, k_s. The pressure under the foundation is p while the settlement is w. If the structure leans by an angle, $d\theta$, due to an increase in the weight, ΔW, the overturning moment, dM_o, caused due to the eccentricity of the weight about the centre of the foundation (Hambly 1985), is

$$dM_o = (W+\Delta W).h.\, d\theta \qquad (9)$$

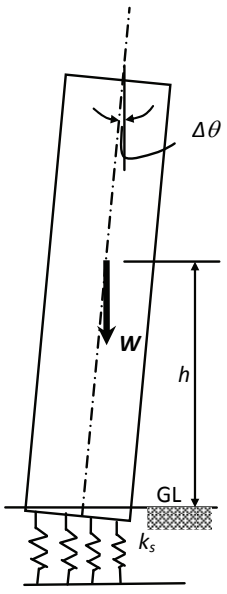

Fig. 20 Tall Structure on Compressible Stratum

The restoring moment, dM_t, generated due to the variation in foundation pressure can be written as

$$dM_t = k_s I_e . d\theta \quad (10)$$

where I_e is the second moment of the area of the foundation about horizontal axis through the centroid. At limiting equilibrium, ΔW = 0, and the following relationship is derived

$$h_e . w_e / r_e^2 = 1 \quad (11)$$

where h_e is the limiting height, w_e-average settlement and $r_e = I_e/A$, A-area of the foundation. Thus the structure starts to lean (leaning instability) when the product of the height to the centre of gravity and the average settlement, w_e $(=W/A.k_s)$, equals the radius of gyration, r_e $(=I_e/A)$. If the structure is loaded non-centrally, an upper bound limit load, W_y, can be estimated in a similar manner, as

$$W_y = k_s . I_y / h_y \quad (12)$$

where I_y is the second moment of the area of the foundation about horizontal axis at edge of foundation and h_y – is the limiting height of the tall structure. Eqs. (11) and (12) demonstrate the effect of the stiffness of the ground on the instability of tall structures. Lancellotta (1993) uses the concept of non-linear moment restraint to explain the leaning instability.

Potts (2003) models the Leaning Tower of Pisa (Figure 21) a typical tall structure, as resting on a uniform deposit of clay defined by its undrained strength, c_u, and shear stiffness, G, with an initial imperfection of 0.5^0 tilt. The undrained strength of the clay was assigned a value of 80 kPa while the value of shear modulus, G, was aried as equal to 10, 100 and 1,000 times the undrained strength. According to conventional theories, the bearing capacity of the foundation of the tower was the same for the three cases considered. If instability is governed by bearing capacity failure of the foundation, all the three analyses indicate the weight of the structure to be the same for the three cases.

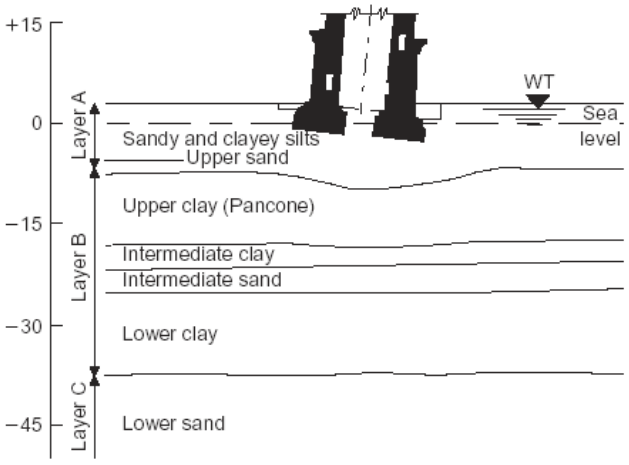

Fig. 21 Soil Profile beneath Pisa Tower

However, if the rotation of the tower is plotted (Figure 22) against its weight, the effect of the relative stiffness of the ground with respect to the undrained strength becomes significant. The weights of the tower for failure are of the order of 65, 120 and 135 MN for G/c_u values of 10, 100 and 1,000. Failure is very abrupt for very stiff soils compared to that of relatively softer soils.

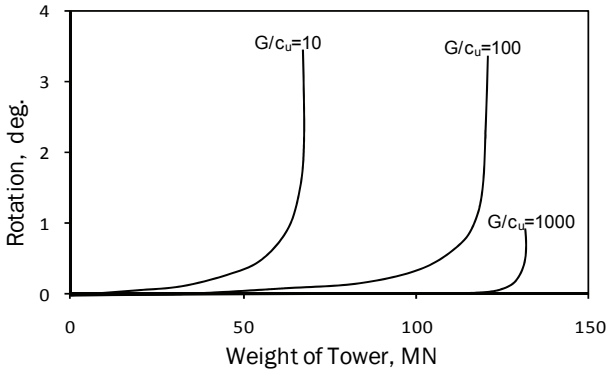

Fig. 22 Rotation with Increase in Weight of Tower (after Potts 2003)

Effect of Thickness of Layer on Consolidation

One Dimensional Problem

The conventional one-dimensional consolidation theory developed by Terzaghi neglects the effect of self weight of the soil and assumes linear relationship of void ratio and effective stress and infinitesimal strain. Richart (1957) reviewed the theory of consolidation and concluded that the effect of considering void ratio as a variable did not significantly change the consolidation-time characteristics of consolidation by vertical flow. The non-linear theory of one-dimensional consolidation developed by Davis and Raymond (1965) considering linear void ratio-log effective stress relationship, is valid only for a thin layer of clay. Gibson et al. (1981) presented a finite strain non-linear one-dimensional consolidation theory for thick homogeneous clays by considering the self weight of soil, variation of void ratio with depth and Lagrangian and convective coordinate system. Analytical solution proposed by Xie et al. (2001) for non-linear one-dimensional consolidation of double layered soil is based on constant effective stress with

depth. Explicit analytical solutions of one-dimensional consolidation of clay are derived by Xie and Leo (2004) for both thin and thick clay layers with mechanics of large strain.

A simple approximate theory of non-linear consolidation is proposed herein (Ayub Khan et al. 2010) for a thick clay layer considering void ratio-log effective stress relationship but assuming coefficient of consolidation (Madhav and Miura 2004) is constant (the coefficient of permeability and the coefficient of volume change are inversely proportional to effective stress), constant thickness of clay layer and constant initial void ratio along the depth but accounting for the variation of initial effective stress with depth as an extension of the non-linear theory of consolidation developed by Davis and Raymond (1965) for a thin layer.

Formulation

A homogeneous saturated clay layer of thickness, H, which is initially fully consolidated under its self weight, (Figure 23), consolidates under a uniformly distributed load, *q,* applied on the top.

Considering linear *e-log σ́* relationship, assuming (1+*e*) constant during consolidation and constant coefficient of consolidation, c_v, (Figure 24) the following equation of consolidation can be derived (Ayub Khan et al. 2010) following Davis and Raymond (1965) in non-dimensional form as

$$\frac{\partial w}{\partial T} = \left[\frac{\partial^2 w}{\partial Z^2} + \frac{1}{10^w .} \frac{\partial w}{\partial Z} \right] \qquad (13)$$

where $w = log_{10}\left(\frac{\sigma'}{\gamma'.H}\right)$, σ'= $(\gamma' z+q-u)$ and γ' is the submerged unit weight of the soil, *Z* and *T* are the normalized parameters; $Z=z/H$ and $T=c_v\, t/H^2$, *σ́* is the effective vertical stress; *t* - time; *u* - the excess pore water pressure and z- depth from surface.

Boundary and Initial Conditions

Two boundary conditions, viz., (i) pervious top impervious base (PTIB) and (ii) pervious top pervious base (PTPB) are considered. Average degree of Settlement, U_s, is

$$U_s = \frac{\int_0^H \log(\frac{\sigma'}{\sigma'_o})\, dz}{\int_0^H \log(\frac{\sigma'_f}{\sigma'_o})\, dz} \qquad (14)$$

Average degree of dissipation of excess pore pressure, U_p, is

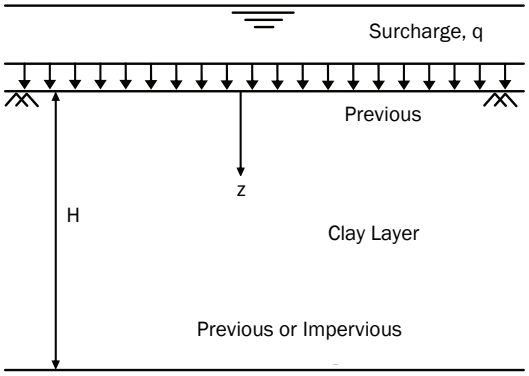

Fig. 23 Consolidation Problem Studied

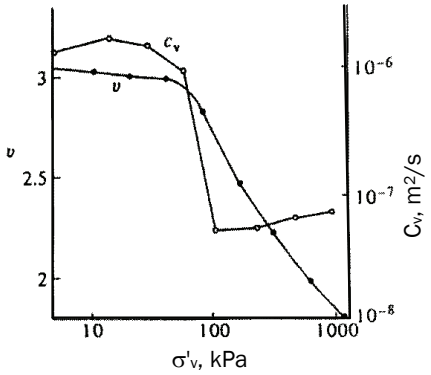

Fig. 24 Variation of Coefficient of Consolidation (c_v) with Effective Vertical Stress (σ'v) (Madhav and Miura, 2004)

$$U_p = \int_0^H \left(1 - \frac{u(z,t)}{u_o}\right) dz \qquad (15)$$

where u_o = q the initial excess pore pressure.

Results and Discussion

Eq. (13) is solved numerically using the finite difference approach. The layer was divided in to hundred sub-layers and convergence ensured. The average degree of settlement for the entire thickness, U_s, by the proposed non-linear theory, is presented in Figures 25 and 26 for PTPB and PTIB cases respectively and compared with the conventional one-dimensional consolidation theory by Terzaghi. The degree of consolidation for a thick layer decreases with increase of q* at all times. The results from the proposed theory agree with the conventional thin layer theory for q* (=q/(γ'H)) ≥ 10,000 (for H tending to zero, thin layer). The degree of consolidation is relatively more in the case of thick layer of clay compared to thin layer for a given load intensity.

Similar observations are made by Gibson et al. (1981). The degree of consolidation increases from 51% to 60% (Figure 25 for PTPB) and from 53% to 71% (Figure 26 for PTIB), for q* decreasing from 10,000 to 1, at a time factor, T_V of 0.197. The theory of consolidation for thin layers thus underestimates the degree of settlement.

The excess pore pressures are computed at different depths and times and the average degree of dissipation of pore pressures for the entire thickness of clay layer is shown in Figures 27 and 28 for different values of q* for PTPB and PTIB respectively along with the results from conventional thin layer theory. The degree of dissipation of pore pressure from non-linear theory is slower than the degree of settlement (Davis and Raymond, 1965, Gibson et al., 1981, and Xie and Leo, 2004). While the degree of settlement is 51% the corresponding degree of dissipation of pore pressure is only 8 % for PTPB (Figure 27) and 53% and 8.30% respectively for PTIB (Figure 28), for q* of 10,000 in thick layers against a value of 50% from linear theory, at

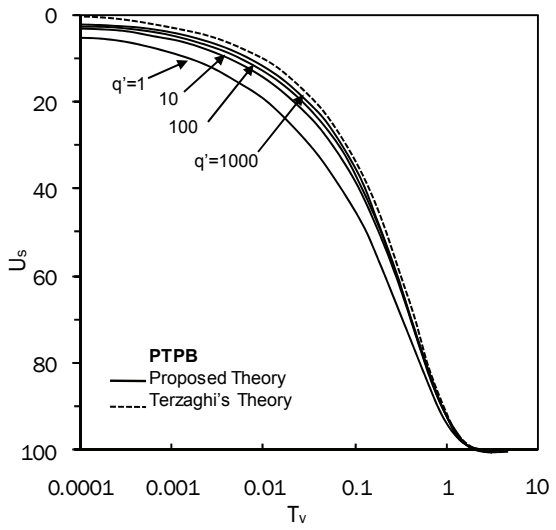

Fig. 25 Degree of Consolidation vs Time Factor (PTPB)

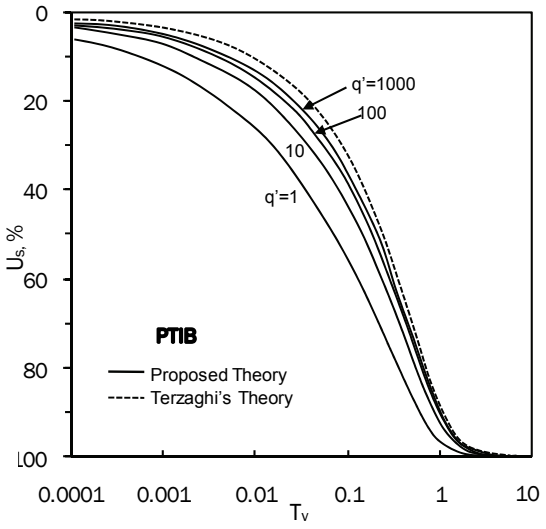

Fig. 26 Degree of Consolidation vs Time Factor (PTIB)

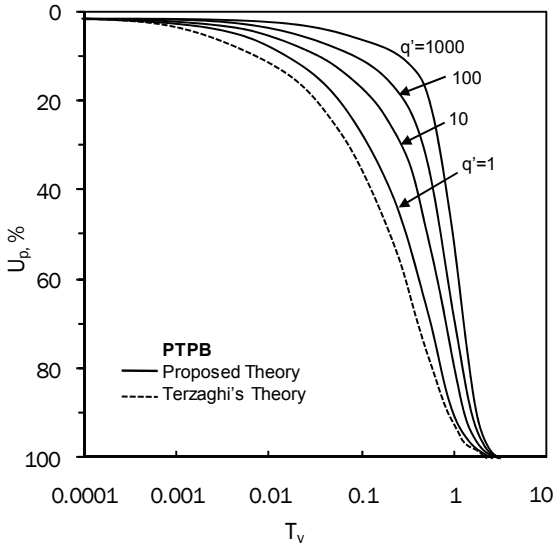

Fig. 27 Average Degree of Dissipation of Pore Pressures vs. Time Factor (PTPB)

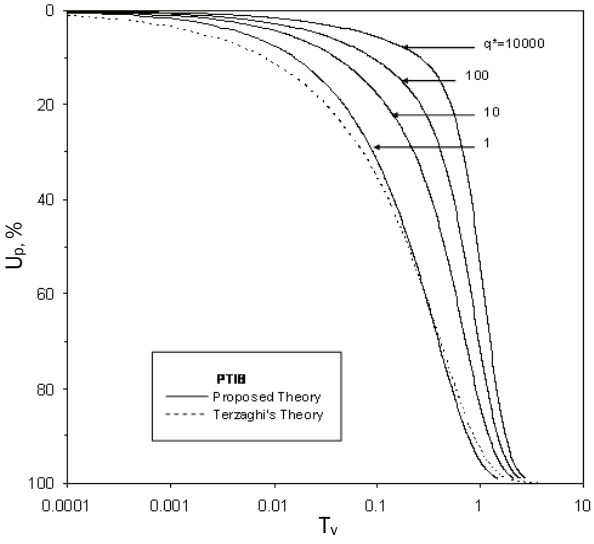

Fig. 28 Average Degree of Dissipation of Pore Pressures vs Time Factor (PTIB)

a time factor of 0.197. The degree of dissipation of pore pressure decreases with the increase of q* as the degree of dissipation of excess pore pressure decreases with the increase of the ratio of final to initial effective stresses as established for the non-linear theory of consolidation (Davis and Raymond, 1965). Thus the conventional thin layer theory over-estimates the degree of dissipation of pore pressures or under-estimates the residual pore pressures of thick layers.

Figures 29 and 30 depict isochrones of excess pore pressure for q*=10 for PTPB and PTIB respectively. The excess pore pressure is relatively large or dissipation of pore pressure is relatively slow at all times according to non-linear theory of consolidation compared to the conventional theory. Interestingly, the isochrones in the case of PTPB are slightly unsymmetrical about the mid depth in contrast to symmetrical isochrones in the conventional linear theory for PTPB boundary conditions. The residual pore pressures are 82% and 78% of q, at depths of 0.2H and 0.8H respectively for q* of 10 at a time factor of 0.20. The corresponding residual pore pressure is 46% of q at the two depths from linear theory.

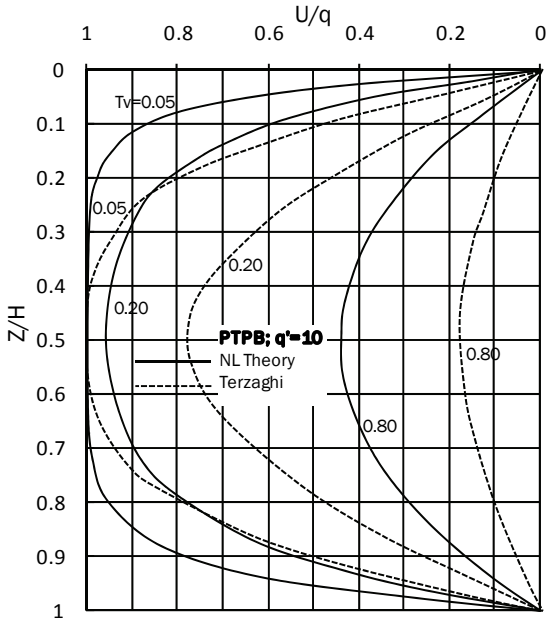

Fig. 29 Excess Pore Pressure Isochrones (PTPB)

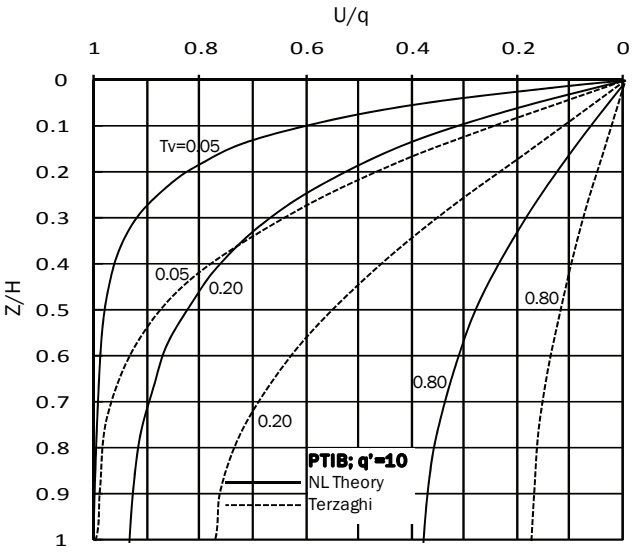

Fig. 30 Excess Pore Pressure Isochrones (PTIB)

Radial Flow - Consolidation into Vertical Drains

Preloading with Prefabricated Vertical Drains (PVDs) is one of the more/most effective methods of soft ground improvement. PVDs shorten the drainage path considerably, promote radial flow and accelerate the rate of consolidation resulting in increased shear strength and reduction of post-construction settlements. Barron's (1948) classical theory is based on the assumptions of small strains, a linear void ratio-effective stress relationship and constant coefficients of volume compressibility (m_v) and horizontal permeability (k_h). However, for a relatively large applied stress range the void ratio is not proportional to effective stress and the coefficients of compressibility and permeability decrease during consolidation. Richart (1957), Basak and Madhav (1978), Hansbo (1979, 1981), Vaid (1985), Lekha et al. (1998), Teh and Nie (2002), Indraratna et al. (2005a and b), Rujikiatkamjorn and Indraratna, (2006) and Conte and Troncone (2009), present more realistic theories of consolidation for radial flow.

Hansbo (1979, 1981) presented a simple solution for radial consolidation with band shaped vertical drains by transforming the drain into an equivalent circular one. Full-scale tests conducted by Bergado et al. (2002) on soft Bangkok clay with PVDs revealed that the degree of consolidation obtained from pore pressure measurements is lower than the corresponding values obtained from settlement measurements. The various modeling aspects of PVDs are comprehensively discussed by Indraratna et al. (2003) along with the evaluation of their effectiveness in practice. Indraratna et al. (2005a and b) developed a theory for consolidation with radial flow using $e - \log\sigma'$ (C_c and C_r) & e – log k_h (C_k) relationships and for different loading increment ratios $(\Delta\sigma' / \sigma_i')$. Zhuang et al. (2005) presented a semi-analytical solution for vertical consolidation of clays with variable compressibility and permeability. The variation of horizontal permeability along the radial direction and the

actual cross sectional shape of band drains are considered in 3D FEM analysis of soft soil consolidation improved by PVDs (Rujikiatkamjorn and Indraratna, 2006). Sathananthan and Indraratna (2006) formulated equivalent plane-strain consolidation equations for radial consolidation in soft soils with PVDs and found good agreement between equivalent plane-strain and axi-symmetric solutions. Indraratna et al. (2007) made a critical review of analytical solutions and numerical analysis of soft clay stabilization with PVDs beneath road and railway embankments. Three and two-dimensional multi-drain finite-element analyses of a case study of a combined vacuum and surcharge preloading with vertical drains is presented by Rujikiatkamjorn et al. (2008). A new technique is developed by Indraratna et al. (2008) to model consolidation by vertical drains beneath a circular loaded area by transforming the system of vertical drains into a series of concentric cylindrical drain wall. Conte and Troncone (2009) developed a simple analytical solution for radial consolidation under time dependent loading. Walker et al. (2009) presented the spectral method for analysis of vertical and radial consolidation in multilayered soils with PVDs assuming constant soil properties within each layer. A theory of non-linear consolidation for radial flow around a vertical drain in a thick deposit of clay is developed herein based on the non-linear theory of consolidation for vertical flow presented by Davis & Raymond (1965).

Vertical Drains

PVDs which are band or strip shaped about 100 mm wide and 4 mm thick, are usually installed in square or triangular arrays (Figure 31a). The strip drain and the zone of influence of each drain are replaced by equivalent circular shapes and the flow pattern around the drain studied considering the flow to be axi-symmetric (Figure 31b). The equivalent diameter of the influence zone, d_e, is 1.13S & 1.05S for square and triangular patterns respectively, where S is the spacing of drains. The equivalent diameter of the drain, d_w, is $d_w = 2(a+b)/\pi$, where 'a' and 'b' are the width and thickness of the PVD respectively.

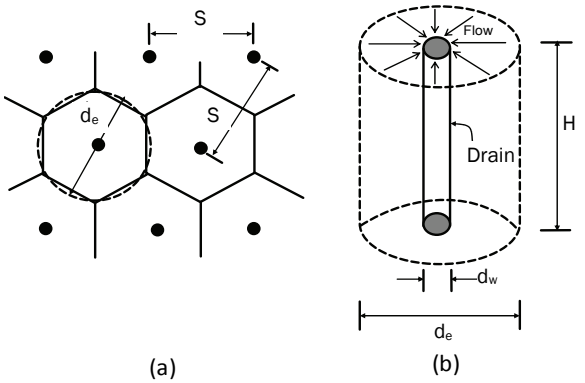

Fig. 31 (a) Triangular Arrangement of PVDs and (b) Flow in Unit Cell

Formulation

The general equation of non-linear consolidation with radial flow (Ayub Khan et al. 2009) in terms of a parameter, *w*, is

$$\frac{\partial w}{\partial t} = c_r\left(\frac{\partial^2 w}{\partial r^2} + \frac{1}{r}\frac{\partial w}{\partial r}\right) \qquad (16)$$

where $w = log_{10}\frac{\sigma'}{\sigma'_f}$ or $w = log_{10}\frac{(\sigma'_f - u)}{\sigma'_f}$, where σ'_f is the final effective stress. '*w*' varies with depth in thick deposits of clay as the initial effective in-situ stress, σ'_o and the final effective stress, σ'_f ($=\sigma'_o + q_0$) vary with depth due to overburden stresses (Figure 32), where q_o is the applied load intensity. Therefore, the thick clay layer of thickness, H is divided equally into *m* thin layers of thickness, $\Delta H = H/m$ (Figure 33) and the differential equation governing the consolidation process of each layer can now be written as:

$$\frac{\partial w_j}{\partial t} = c_r\left(\frac{\partial^2 w_j}{\partial r^2} + \frac{1}{r}\frac{\partial w_j}{\partial r}\right) \qquad (17)$$

where the subscript j refers to the layer number and $w_j = w_j$ (r, t) of the j^{th} layer. Even though the initial and final effective stresses are different in each layer, the flow in each layer is assumed to be purely radial and independent of the flows in the adjacent layers.

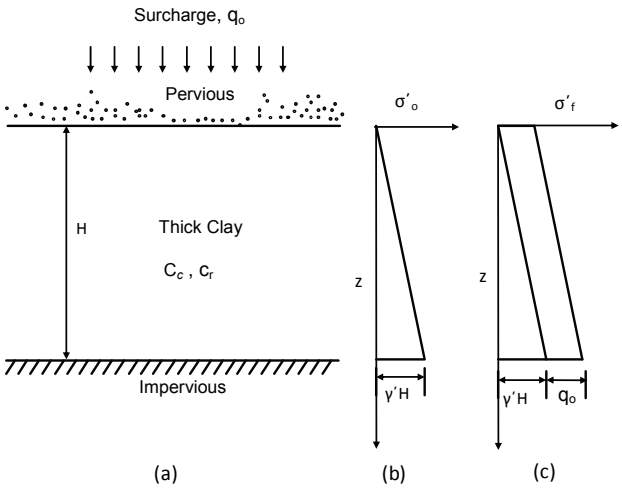

Fig. 32 (a) Thick Clay Loading Condition; (b) Initial in-situ Stress (σ'_o) Distribution; c) Final Stress (σ'_f) Distribution

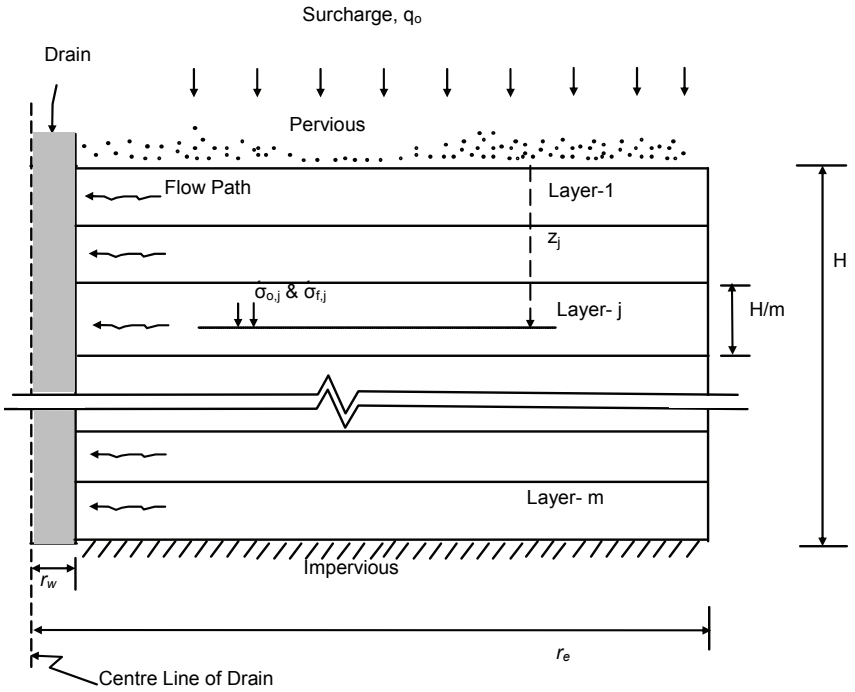

Fig. 33 Radial Flow in Clay Layers

$$U_{S,j} = \frac{\int_{r_w}^{r_e} (e_o - e)\, 2\pi\, r\, dr}{\int_{r_w}^{r_e} (e_o - e_f)\, 2\pi\, r\, dr} \qquad (18)$$

where $w_j = log_{10}\frac{\sigma'_j}{\sigma'_{f,j}}$, $w_{o,j} = log_{10}\frac{\sigma'_{o,j}}{\sigma'_{f,j}}$ and the initial or original effective in-situ stress at the layer j, $\sigma'_{o,j} = \gamma'.z_j$, z_j the depth of the layer j.

Average degree of consolidation for the entire thickness,

$$U_s = \frac{\sum_{j=1}^{m} U_{s,j}.(\Delta H)_j}{H} \qquad (19)$$

Normalized average excess pore pressure over the radial distance at the layer j is:

$$U*_{avg,j} = \frac{\int_{r_w}^{r_e} u_j\, 2\pi\, r\, dr}{\int_{r_w}^{r_e} u_o\, 2\pi\, r\, dr} \qquad (20)$$

Degree of dissipation of average excess pore pressure at the layer j is

$$U_{P,j} = (1 - U*_{avg,j}) \qquad (24)$$

Average degree of dissipation of excess pore pressure for the entire thickness is

$$U_P = \frac{\sum_{j=1}^{m} U_{P,j}.(\Delta H)_j}{H} \qquad (21)$$

Eqn. (13) is identical in form to that of the conventional Barron's radial consolidation theory and can be solved in the same way with the boundary conditions that are the same in terms of *u* and *w*.

Initial and Boundary Conditions

For t = 0 and $r_w \le r \le r_e$, $u_j(r,0) = (\sigma_{f,j} - \sigma_{0,j})$ or $w_j(r,0) = w_{0,j}$ ® = $\log_{10}(\sigma'_{0,j}/(\sigma'_{f,j})$. For t > 0 at $r = r_w$, $u_j(r_w,t) = 0$ or $w_j(r_w,t) = 0$ and at $r = r_e$ $\delta u_j/\delta r = 0$ or $\delta w_j/\delta r = 0$ for j = 1, 2, 3, ...m. The radius of influence zone, $r_e = 0.5d_e$ and radius of equivalent drain, $r_w = 0.5d_w$. Equation (13) in non-dimensional form is

$$\frac{\partial w_j}{\partial T} = \left(\frac{\partial^2 w_j}{\partial R^2} + \frac{1}{R}\frac{\partial w_j}{\partial R}\right) \qquad (14)$$

where $R = r/d_e$ and $T = c_r t/d_e^2$.

Results and Discussion

A thick clay layer of thickness, H, is divided into 'm' (=20) layers of equal thickness, $\Delta H = H/m$, as shown in Figure 33. The numerical analysis is carried out for each layer independently using the corresponding σ_f/σ_o and the results obtained in terms of degree of settlement, U_s, and excess pore pressures, u. Variations of these results along the depth and radial distance are studied. As non-linear consolidation is mainly influenced by the stress ratio, σ'_f/σ'_o, the variation of σ'_f/σ'_o with depth is shown in Figure 34 for different values of normalized applied load intensity, $q^*_o=q_o/(\gamma.H)$. The stress ratio, σ'_f/σ'_o decreases sharply from values as high as 21 to 121 near the surface (at z=0.025H) to 6.30 to 33 at z=0.1H for values of q^*_o increasing from 0.50 to 3.0. The decrease of σ'_f/σ'_o with depth is very sharp as the initial effective stress is very small near the top. The decrease of σ'_f/σ'_o with depth is significant for depths in the range 0.1H to 0.4H, the values reducing to about 2 to 8.5 at z=0.4H for values of q^*_o increasing from 0.50 to 3.0, and negligible for z>0.4H for all q^*_o. Hence, the effect of non-linear consolidation in a thick clay layer can be pronounced at shallow depths compared to that at greater depths. Increases in q^*_o can be either due to increase of load intensity, q_o for a given thickness, H, or due to decrease of thickness of clay deposit for a given load intensity. In either case, only the non-dimensional stress ratio, σ'_f/σ'_o, influences the rate of consolidation and not the thickness of the deposit or the magnitude of loading individually.

The degree of settlement, U_s, is determined for different layers along the depth for various q_o* values for different values of *n* ranging from 5 to 40 and shown in Figure 35. The degree of settlement is identical at all the layers in given thick clay for all values of *n* and q^*_o. The degree of settlement obtained from the present non-linear theory is identical to that from the linear theory (Barron 1948) for free strain case. The degree of settlement, U_s, is independent of σ'_f/σ'_o and varies only with *n* as is the case for vertical flow (Davis and Raymond 1965). The degree of settlement decreases with increase of *n* since it takes relatively long time for dissipation of pore pressure for larger radial distances. U_s decreases from 58% to 24.8% for *n* increasing from 5 to 40 at a time factor of 0.10. The excess pore pressure varies with the radial distance being zero at the drain surface and maximum at the boundary of unit cell. Therefore, the average excess pore pressure, $u_{avg}(z)$ is determined along the radial distance for $r=r_w$ to r_e at different layers for various *n* and q^*_o values. Accordingly, at each layer the normalized average excess pore pressures, $U^*_{avg}(z) = (u_{avg}(z)/u_o).100$ are obtained, where u_o is the initial excess pore pressure ($=\sigma_f - \sigma_o$). Average normalized excess pore pressures for the entire thickness or for all the layers, U^*_{avg} is obtained and the degree of dissipation of average excess pore pressure for the entire thickness, $U_p = (100-U^*_{avg})$ is presented in

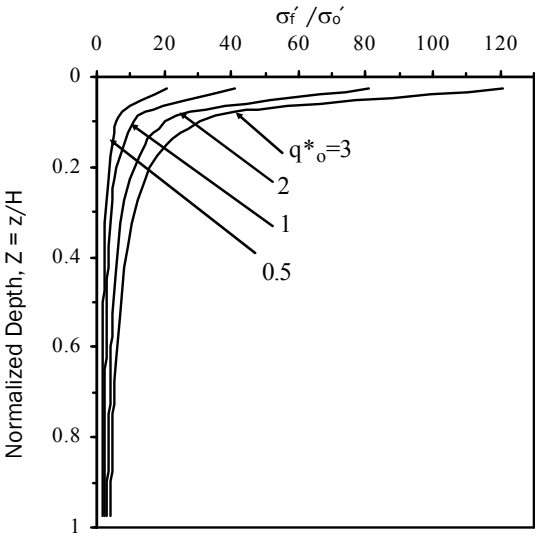

Fig. 34 Variation of σ_f'/σ_o' with Depth

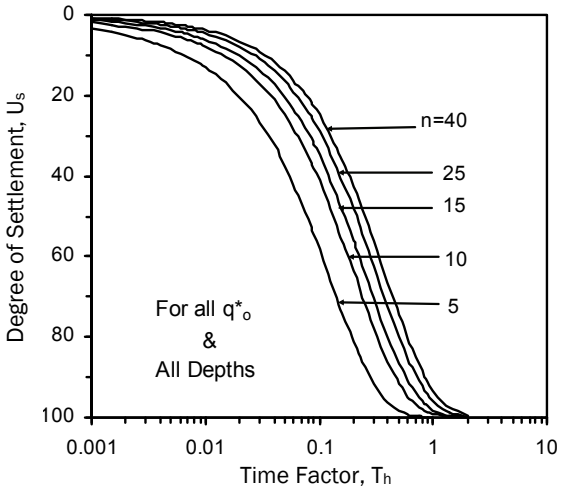

Fig. 35 U_s versus T_h for both Linear and Non-Linear Theories – Effect of 'n'

Figure 36 for n=15 along with the degree of settlement, U_s. While the degree of settlement is independent of q^*_o, the degree of dissipation of pore pressure, U_p is sensitive to q^*_o values. The degree of dissipation of average excess pore pressure decreases with the increase of q^*_o. At T_h equal to 0.20, the degree of dissipation of average pore pressure decreases from about 45% for q^*_o of 0.50 to about 33% for q^*_o of 2 while the degree of settlement is 55.90%. Thus for a given thickness of clay deposit, the increase of load intensity, q_o results in decrease of degree of dissipation of average excess pore pressure or for a given load intensity the decrease of thickness of clay deposit results in decrease of degree of dissipation of average excess pore pressure.

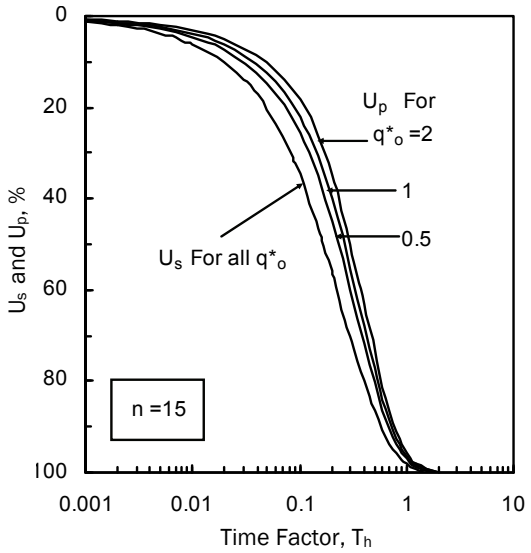

Fig. 36 Variation of U_s and U_p with T_h

Figure 37 shows variation of degree of settlement, U_s and normalized average excess pore pressure, $U^*_{avg}(z)$ with time at a depth, z =0.5H for *n*=15 and q^*_o ranging from 0.5 to 4. While the degree of settlement is independent of the q^*_o and depth, the normalized average excess pore pressures at the depth are sensitive to q^*_o values. The average excess pore pressure increases or the degree of dissipation of average excess pore pressure at any depth, $U_p(z)$ = (100-$U^*_{avg}(z)$) decreases with the increase of q^*_o. For example, at 90% degree of settlement, i.e. at T_h equal to about 0.60, the degree of dissipation of average pore pressure decreases from about 88% for q^*_o of 0.50 to about 80% for q^*_o of 4. Similarly, at 60% degree of settlement, i.e. at T_h equal to about 0.22, the degree of dissipation of average pore pressure decreases from 51.5% for q^*_o of 0.50 to about 35% for q^*_o of 4.

The normalized average excess pore pressure, $U^*_{avg}(z)$ = $(u_{avg}(z)/u_o)$.100 at other depths is also determined and its variation with time is shown in Figure 38 for *n*=15 and q^*_o=1 along with the degree of settlement. The excess pore pressure is relatively high at shallow depths where the σ'_f/σ'_o ratio is relatively high compared to the values at greater depths. For example, at 90% degree of settlement, i.e. at T_h equal to about 0.60, $U^*_{avg}(z)$ decreases from about 30% at a depth of 0.025H to 12% at a depth of 0.975H. Similarly, at 60% degree of settlement i.e. at T_h equal to about 0.22, $U^*_{avg}(z)$ decreases from about 79% at a depth of 0.025H to 49% at a depth of 0.975H, The differences in $U^*_{avg}(z)$ from different depths are relatively more during the intermediate stages of consolidation compared to the final stage of consolidation. The importance of the above finding is that when large load is applied on soft

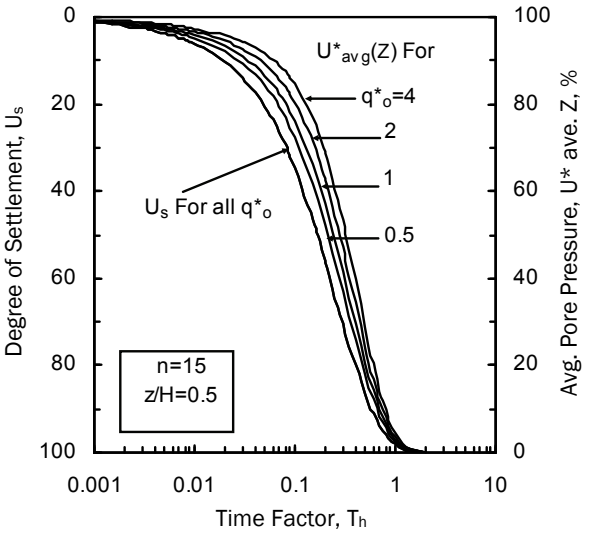

Fig. 37 Variation of U_s & $U^*_{avg}(z)$ with T_h -- Effect of Load Intensity

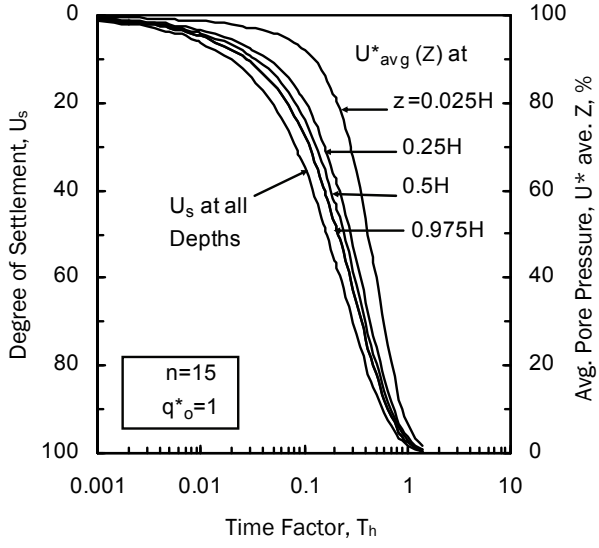

Fig. 38 Variation of U_s & $U^*_{avg}(z)$ with T_h -- Effect of Depth

ground, the possibility of shallow seated rotational bearing failure is to be examined in view of the large residual pore pressures at these depths over longer periods of time.

The residual average excess pore pressure, u_{avg} (z), at different depths of the thick clay are computed for various values of q^*_o, *n* and T_h and the normalized average excess pore pressures, U^*_{avg} (z) = (u_{avg}(z)/u_o).100, are presented in Figure 39 for *n*=15 at time factor, T_h=0.20 along with the results of linear theory. The remarkable phenomenon observed is that average pore pressure values from the non-linear radial consolidation theory vary with depth in contrast to the depth-independent U^*_{avg} values of linear theory. U^*_{avg}(z) varies from about 77% to 89% near the surface to about 49% to 63% near the bottom for values of q^*_o ranging from 0.50 to 4.0 against a constant value of about 44% through out the depth in linear theory. The difference between the pore pressures of non-linear and linear theory is relatively large at shallow depths due to large values of σ'_f/σ'_o compared to those at greater depths. This difference increases with increase of q^*_o. Moreover, at shallow depths the variation of pore pressure with depth is relatively very large compared to that at greater depths due to sharp variation of σ'_f/σ'_o at shallow depths. While the excess pore pressures in the linear theory are independent of, q^*_o, the pore pressures according to non-linear theory are dependent on q^*_o as the variation of q^*_o influences the ratio σ'_f/σ'_o. The average pore pressure increases from about 52% to 69% at mid-depth of clay for q^*_o increases from 0.5 to 4. The residual average excess pore pressures thus are underestimated in the conventional linear theory. In view of the above, instead of applying the entire preload instantaneously on the soft ground, it may be applied in increments with proper time lag to allow quicker dissipation of pore pressures and gain of shear strength.

The effect of increase of *n* on the distribution of the normalized average excess pore pressure, U^*_{avg} (z), with depth is shown in Figure 40 for q^*_o=1, T_h=0.20 and *n* from 5 to 40. The variation of U^*_{avg} (z) is relatively significant at shallow depths for all the *n* values compared to the variation at greater depths. As expected, at any given depth, U^*_{avg}(z) increases with increase of *n* since the points farther from the drain take relatively longer times to dissipate the excess pore pressures. U^*_{avg} (z) increases from 28% to 70% at mid depth of clay for *n* increasing from 5 to 40.

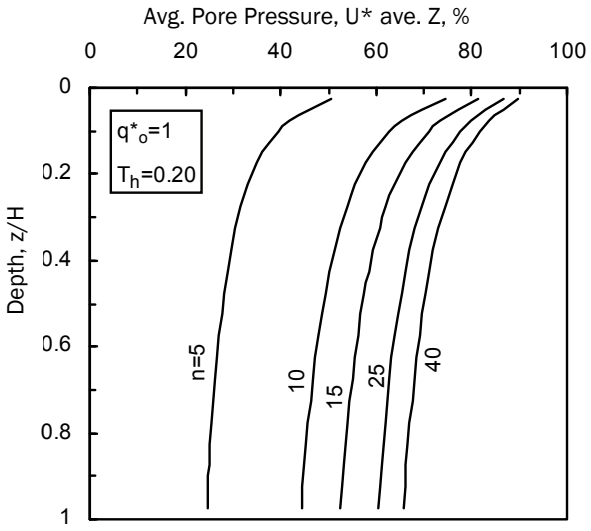

Fig. 40 Variation of U^*_{avg}(z) with Depth—Effect of *n*

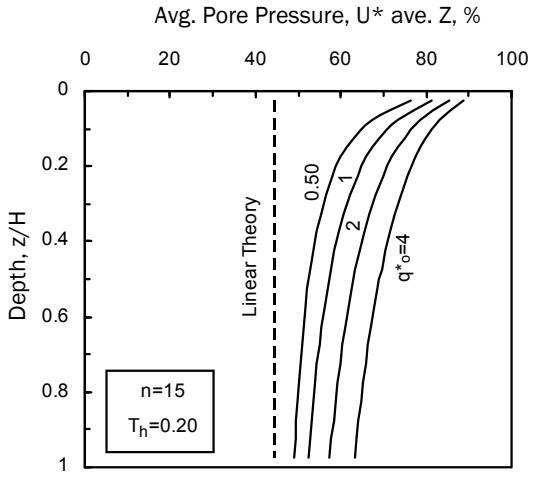

Fig. 39 Variation of U^*_{avg}(z) with Depth—Effect of Load Intensity

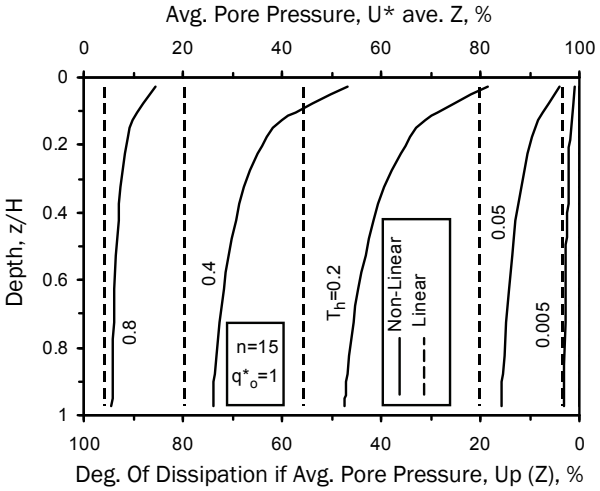

Fig. 41 Variation of U^*_{avg}(z) with Depth—Effect of Time

Variations of the normalized average excess pore pressure, U^*_{avg} (z) and degree of dissipation of average excess pore pressure, $U_p(z) = (100-U^*_{avg}(z))$ with depth and time are shown in Figure 41 for *n*=15 and q^*_o=1. Values from linear theory which remain constant with depth are also shown. At any depth, the degree of dissipation of average excess pore pressure, $U_p(z)$, is relatively smaller in the non-linear theory compared to that in the linear theory. The expulsion of pore water depends on permeability of the soil and the permeability decreases during consolidation due to increase of effective stress. The variation of permeability of the soil during consolidation is considered in the present non-linear theory.

The dissipation of pore pressures is relatively very slow at shallow depths compared to that at greater depths in view of the large ratio of final to initial stress at shallow depths. For example, at a time factor of 0.20, the degree of dissipation of average pore pressure in the non-linear theory increases from 18.57% near the surface (z=0.025H) to 47.40% near the bottom (z=0.975H) while it is 55.9% constant with depth in the linear theory. Obviously, at the initial stage of consolidation (T_h=0.005) and towards the end (T_h=0.80), the difference in the degrees of dissipation of average excess pore pressures of the two theories is relatively less compared to those at intermediate stages of consolidation. Near the surface at a depth of z=0.025H, the difference in the degrees of dissipation of average excess pore pressures of the two theories is only 2.70% for T_h of 0.005, the difference increasing to 37.30% for T_h of 0.20 and decreases to 10.40% towards the end at T_h of 0.80.

The distribution of normalized excess pore pressure at any radial distance and depth, $U^*(r/r_w, z) = (u(r/r_w,z)/u_o.100)$ with depth at different radial distances is presented in Figures 42(a) and (b) (next page) for time factors of 0.05 and 0.20 respectively for n=15 and q^*_o=1. The residual pore pressures are relatively small being less than 20% close to the drain. The excess pore pressures vary between 84% to 99% in the outer half of the unit cell (i.e. $r > r_w+0.5(r_e-r_w)$) while the variation is relatively sharp ranging from 97% to 0% in the inner half of the unit cell at time factor of 0.05, The pore pressures are nearly constant at all depths farther from the drain compared to the sharp variation in the values in the middle of the unit cell at all the times. Thus the effect of thickness of the deposit is significantly more at half the distance from the drain to the edge of the unit cell. The variations of pore pressures at different radial distances with depth at T_h equal to 0.2 is similar to those for T_h equal to 0.05 but the magnitudes of the pore pressures are lesser as can be expected at larger times.

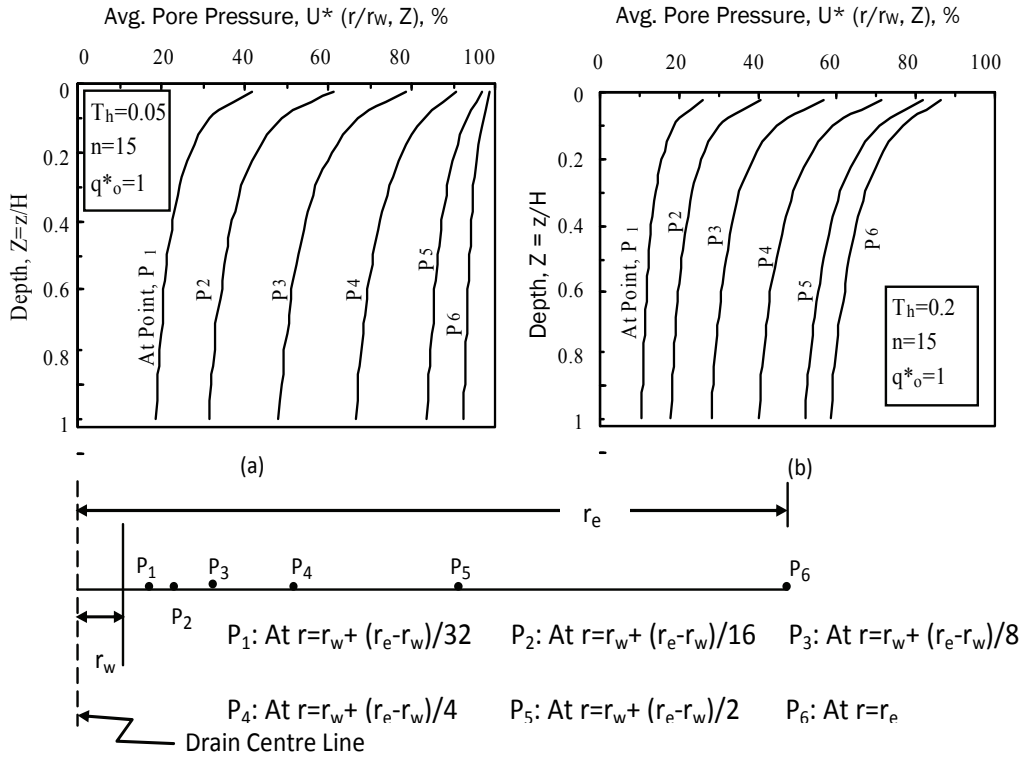

Fig. 42 Pore Pressure Distribution with Depth at (a) T_h=0.05 and (b) T_h=0.2

Figure 43 shows the pore pressure variation with radial distance at different depths for q^*_o=1, *n*=15 and T_h=0.20. The excess pore pressures are relatively large at shallow depths wherein the stress ratio is extremely large but decrease with depth since the ratio of final to initial stress decreases with increase of depth. The pore pressure variation with radial distance, r, is relatively more significant in the upper half of the deposit compared to that in the lower half. At r=r_e and time factor of 0.20 the pore pressures decrease from about 87% near the surface to 63% at z=0.5H and to about 58% near the bottom of the layer. The pore pressure variation is relatively more significant at points close to the drain compared to the variation at farther points as the dissipation of pore pressure is rapid close to the drain. The pore pressure varies from 0 to 47% in the inner one-third of the unit cell at z=0.5H, and from 47% to 63% in the remaining two-thirds of the unit cell.

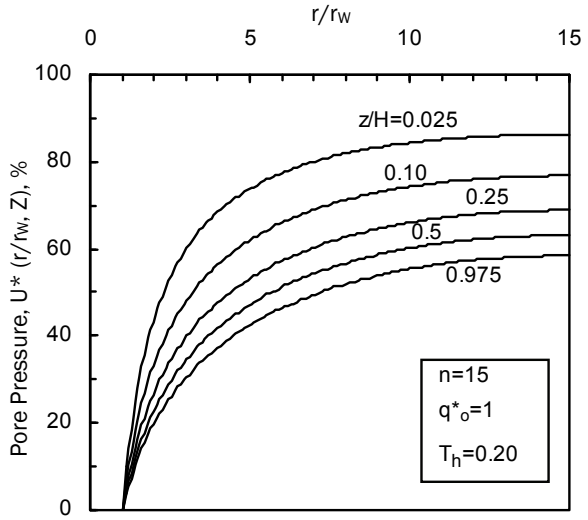

Fig. 43 Variation of Pore Pressures with Radial Distance—Effect of Depth

The effect of intensity of loading, q^*_o, on the variation of excess pore pressure with radial distance at a depth of z=0.5H is shown in Figure 44 for *n*=15 and T_h=0.20. The pore pressure increases from about 50% to 68% at the centre of the unit cell and from 58% to 75% at the edge of the unit cell for q^*_o increasing from 0.5 to 4. The excess pore pressure at any radial distance increases with increase of load intensity as it leads to a corresponding increase of the stress increment ratio, σ'_f / σ'_o.

Figure 45 shows the effect of time on excess pore pressure, U*(r/r_w, z) distribution along a radial line at mid depth of the layer for q^*_o=1 and *n*=15. The pore pressure variation along the radial line is relatively considerable in the initial stages of consolidation. At a time factor of 0.10 the pore pressure varies from zero at the drain to 83.25% at the farthest end of zone of

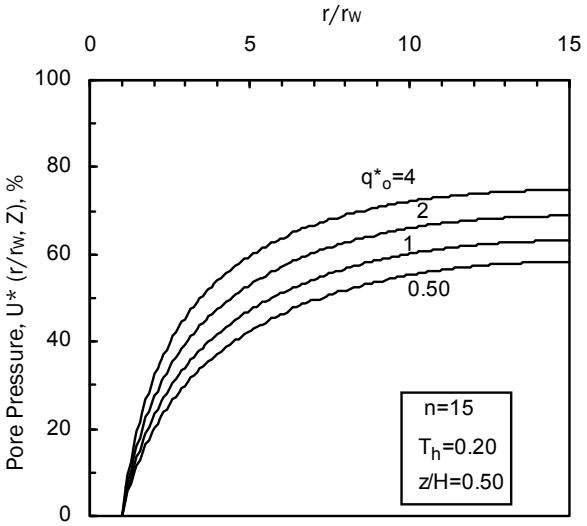

Fig. 44 Variation of Pore Pressures with Radial Distance—Effect of Load Intensity

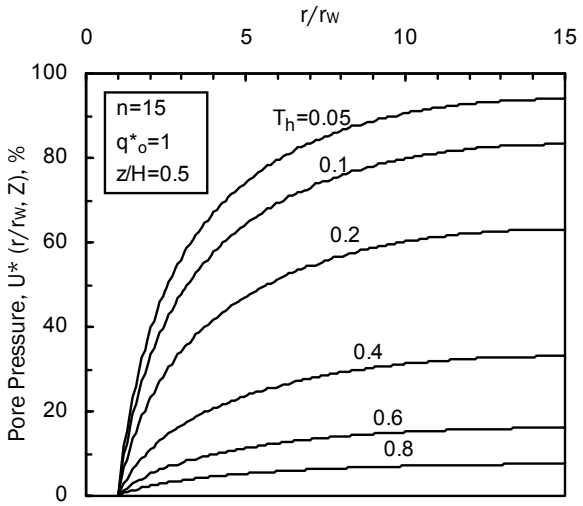

Fig. 45 Variation of Pore Pressures with Radial Distance—Effect of Time

influence. However, the pore pressure variation becomes as expected relatively negligible in the later stages of consolidation (T_h >0.6), the variation being only from 0 to 12 % at T_h=0.6. The pore pressure distributions along the radial line at mid depth of the layer for q_o*=1, at T_h=0.20 and for various *n* values are shown in Figure 46. The maximum excess pore pressure at the end of zone of influence increases with increase of *n* as the farther points take relatively longer times to dissipate the pressures.

The pore pressure increases from 33.50% to 74.60 % for *n* increasing from 5 to 40 for the above loading and time at mid depth of soil. The excess pore pressures, $U^*(r/r_w, z)$ are nearly the same at small values of r/r_w for different *n* values and the values diverge at farther points because of slower dissipation for larger spacing of the drains $U^*(r/r_w, z)$ increasing from 33.50% to 43% for *n* increasing from 5 to 40 at r/r_w=5.

Inelasticity and Rotation of Tall Structures

Tall structures are very often subjected to large moments due to wind or other dynamic forces which can cause the structures to tilt as a whole. All the analyses so far available assume that the modulus of deformation of the soil under compression is the same as that for stress removal or unloading. However it is well known that these two moduli are not the same. During compression, the soil undergoes both plastic and elastic deformations, while only the elastic part of the total deformation is recovered during unloading. Consequently, the modulus for unloading is much larger than that for compression. Numerous experimental results from plate and pile load tests have established this type of behaviour of soil.

Rotation of rigid footing due to moment is studied by few researchers. Most of the relationships are obtained on the basis of Winkler (one parameter) or the elastic continuum models based on Boussineq's or Mindlin's expressions. Weismann (1972) derives expressions using Winkler's model, for tilt of rigid foundations of rectangular and circular shapes. Rotation due to moment loading on smooth, rigid circular footing is obtained by Borowicka (1943) for semi-infinite soil. Moment loading on rigid, rectangular footing on elastic half – space is considered by Lee (1962) and Richart and Whitman (1967). The case of eccentric loading on smooth, rigid, annular footing on elastic half space is investigated by Hara et al. (1975), Egorov and Vronsky

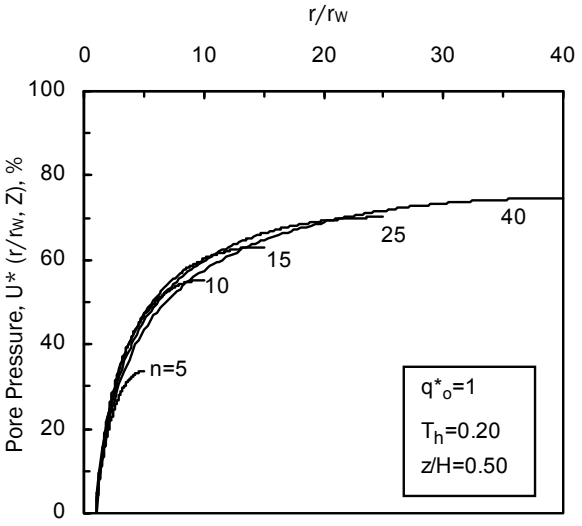

Fig. 46 Variation of Pore Pressures with Radial Distance—Effect of *n*

(1980) and Egorov et al. (1979, 1980), Georgiadis and Butterfield (1988) and Gazetas (1998). Poulos and Davis (1974) compile available solutions on moment – rotation relationships for elastic ground. All these studies are based on perfectly elastic soil, i.e., the moduli in compression and unloading are equal. In the present work, moment- rotation relationship of soil- rigid footing system subjected to moment are found out using different types of soil structure interaction models considering soil modulus in unloading to be different from that in compression.

Statement of Problem

A rigid footing resting on the surface of ground and subjected to an applied moment, *M*, is considered (Figure 47(a)). The ground below one part of the footing undergoes compression while the other part undergoes unloading or stress reversal. A modular ratio, R_k, is

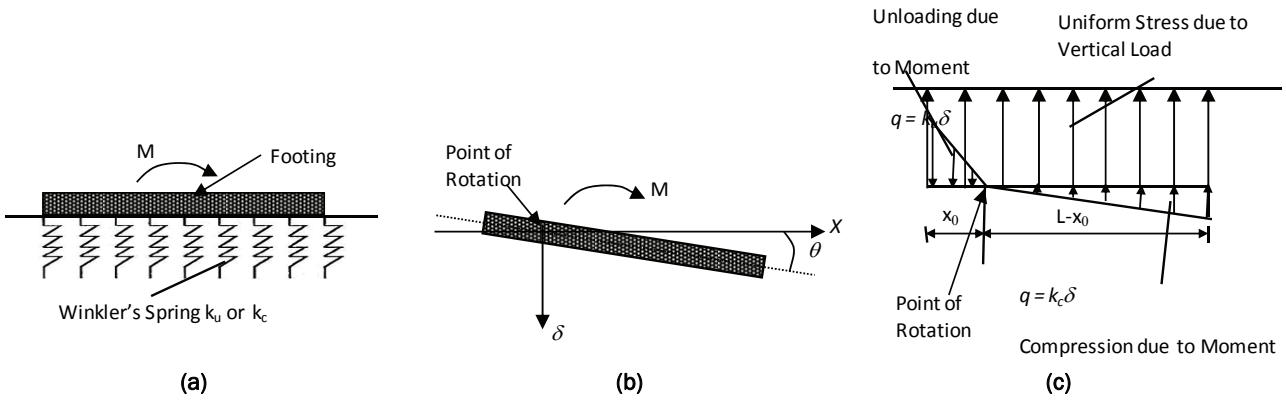

Fig. 47 (a) Winkler Model of Soil-Structure Response
(b) Moment Loading on Foundation (c) Contact Pressure due to Moment on Rectangular Footing

defined as $R_k = k_u/k_c$, where k_c and k_u are moduli of subgrade reaction in compression and unloading respectively.

Analysis

The foundation - soil response is represented by a series of independent springs in Winkler model. The footing rotates about an axis passing through the center of the contact area with the soil due to symmetry in pressure distribution (elastic response) for R_k = 1. However, the axis of rotation shifts away from the compression zone towards the unloading zone for R_k > 1.0 to compensate for the larger subgrade modulus in unloading. The analysis consists of mainly two steps, viz., force equilibrium and moment equilibrium equations and is given in Madhav et al. (2009).

Rectangular Footing

A rectangular footing of width, B, and length, L, subjected to moment, M and its deformation response are shown in Figures 47(a) and (b). The distance to the axis of rotation from the left edge of footing (Figure 47(c)) is x_0. The footing rotates through an angle θ due to the applied moment, M. The stress on the compression side (Figure 47(c)) is $k_c\delta$ where $\delta=\theta.x$ is the soil deformation x- the distance from the axis of rotation. Similarly, the stress on the footing is $k_u.\delta$ or $k_u.\theta.x$ on the unloading side. Negative sign indicates unloading. Since a footing subjected to only moment is considered no vertical force acts on the footing. Force and moment equilibrium equations lead to the estimation of rotation, θ, as expressed as

$$\theta = \frac{M\, I_{\theta wr}}{(k_c BL^3)} \qquad (15)$$

where $I_{\theta wr} = 3/\{(1-X_0)^3 + R_k X_0^3\}$, $X_0 = x_0/L$ and $I_{\theta wr}$ - influence coefficient, a function of R_k.

Circular Footing

The corresponding equation for a circular footing (Figure 48) following numerical integration is

$$\theta = M^* I_{\theta wc} \qquad (16)$$

where $M^*=M/k_c d^4$, d - the diameter of the footing, $I_{\theta wc}$ - a function of $X_0=x_0/R$ and R_k.

Annular Footing

R_1 and R_2 are respectively the inner and the outer radii as shown in Figure 49. The expression for θ for an annular footing is

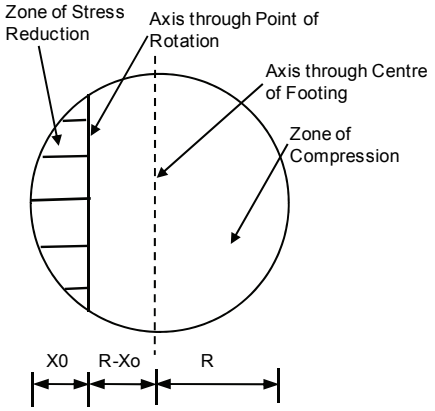

Fig. 48 Circular Footing

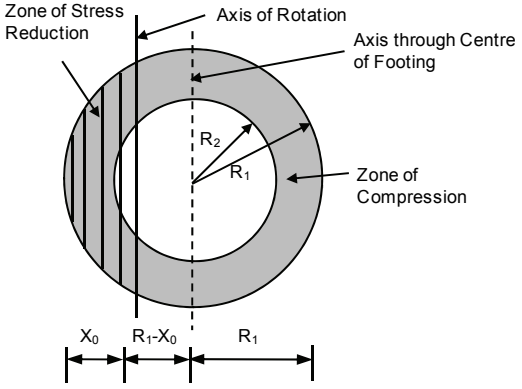

Fig. 49 Annular Footing

$$\theta = M^* I_{\theta wa} \qquad (17)$$

where $M^* = M/k_c d_1^4$, d_1 is the outer diameter of annular footing and $I_{\theta wa}$ - a function of R_k and $n = R_2/R_1$ - the ratio of inner to outer radii, termed the annular ratio.

Non-linear Response

The stress-deformation characteristics based on hyperbolic model is expressed as

$$q = \frac{k_c \delta}{1 + \frac{k_c \delta}{q_{ult}}} \qquad (18)$$

where q is the average vertical stress on the soil, δ - the displacement of soil-foundation system, q_{ult} - the

ultimate stress of soil, k_c- the initial slope of the stress-displacement response of soil. The non-linear (hyperbolic) response of the soil is considered for the zone of soil which is in compression due to the applied moment (Figure 50(a)). Linear stress-deformation relationship is assumed for unloading.

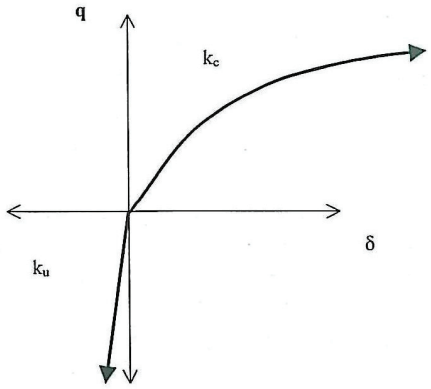

Fig. 50 (a) Stress-Deformation Response for Nonlinear Winkler Model

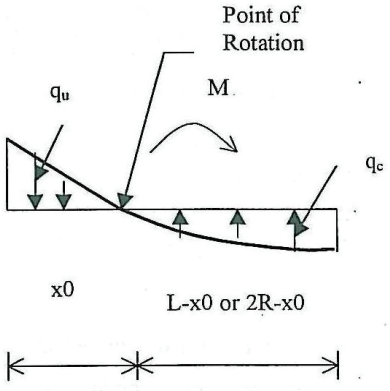

Fig. 50 (b) Contact Pressure Distribution below Footing

Rectangular Footing subjected to Moment Loading only

The contact pressure distribution is shown in Figure 50(b). The force and moment equilibrium equations on simplification are

$$\frac{\beta}{(\theta * R_k)}\left[(1-x_0)-\left(\frac{\beta}{\theta}\right)\ln\left\{1+\frac{\theta}{\beta}(1-x_0)\right\}\right]-\frac{x_0^2}{2}=0 \qquad (19)$$

$$\frac{\beta^2}{\theta^2}\left[\frac{\left\{1+\frac{\theta}{\beta}(1-x_0)\right\}^2}{2}-2\left\{1+\frac{\theta}{\beta}(1-x_0)\right\}+\ln\left\{1+\frac{\theta}{\beta}(1-x_0)\right\}-0.5+2\right]+\frac{R_k\theta x_0^3}{3}=\frac{M}{L^3k_cB} \qquad (20)$$

where $\beta = q_{ult}/k_c.L$ - a dimensionless parameter.

Effect of Vertical Load prior to Application of Moment

If vertical load acts before the application of moment, the displacement has two components: uniform settlement and rigid body rotation. Subgrade modulus, k_c, for rotation would be different from k_{ci}, the initial subgrade modulus. The moment-rotation relationship is estimated using an appropriate tangent subgrade modulus, k_{ct} (Figure 50(c)). With q - the applied vertical stress prior to moment loading and δ^q - the corresponding displacement.

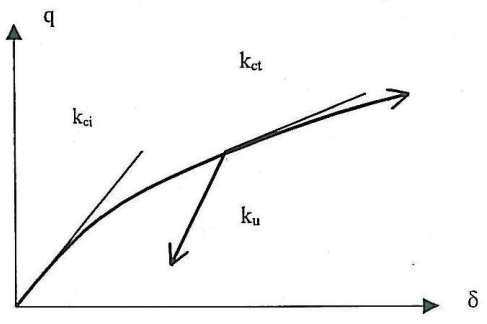

Fig. 50 (c) Stress-Deformation Response for Applied Vertical Load prior to Moment

$$q = \frac{k_{ci}\delta'}{1+\frac{k_{ci}\delta'}{q_{ult}}} \Rightarrow \delta' = \frac{q/k_{ci}}{1-\frac{q}{q_{ult}}} \quad (21)$$

$$\text{or} \quad \delta^* = \delta'/L = \frac{q^*\beta}{1-q^*} \quad (22)$$

where $q^*=q/q_{ult}$ and

$$k_{ct} = \left(\frac{dq}{d\delta}\right)_{\delta=\delta 1} = \frac{k_{ci}}{\left(1+\frac{k_{ci}\delta 1}{q_{ult}}\right)^2} = \frac{k_{ci}}{\left(1+\frac{\delta^*}{\beta}\right)^2} = \frac{k_{ci}}{m} \quad (23)$$

The force and moment equilibrium equations are

$$\frac{\beta}{\theta}\left[1-x_0-\frac{m\beta}{\theta}\ln\left\{1+\frac{\theta}{m\beta}(1-x_0)\right\}\right]-\frac{R_k X_0^2}{3}=0 \quad (24)$$

$$\frac{m^2\beta^3}{\theta^2}\left[\frac{1}{2}f^2-2f+\ln(f)-\frac{1}{2}+2\right]+\frac{R_k\theta X_0^3}{3}=\frac{M}{k_{ci}BL^3} \quad (25)$$

where $f = 1+ (1-x_0).\theta/\beta m$.

Circular Footing with Moment Only

Moment - rotation relationship for circular footing (Figure 48) on nonlinear foundation [Figure 50(c)] is obtained from the corresponding force and moment equilibrium equations (Madhav et al. 2009). The terms are integrated numerically to determine X_0 and I_θ. Table 1 lists the parametric values used in the present analysis.

Results and Discussion

The effect of inelastic stiffness ratio, R_k, on the moment-rotation relationships of rigid footings subjected to moment loading are obtained based on Winkler model. Figure 51 presents the variation of X_0, the distance to the axis of rotation for rectangular and circular footings with R_k. The axis of rotation passes through the midpoint of the length of rectangular or diameter of the circular footing, i.e. X_0=0.5 for R_k=1. The axis of rotation shifts towards the zone of stress reduction with increasing inelasticity or R_k values. The rate at which the axis of rotation shifts with increase in R_k is quite high for R_k<5 for both rectangular and circular footings. The rate of decrease of X_0 with R_k decreases gradually for R_k>5. Though the rate of shift of the axis of rotation is nearly the same for both types of footings for R_k<2, the rate of decrease is somewhat faster for rectangular footing for higher R_k. For example, at R_k=20, X_0 shifts by about 32% of its length for rectangular footing, while it is only 25% of the diameter for circular footing.

Figure 52 depicts the variation of I_θ with R_k for circular and rectangular footings. I_θ decreases with increase in R_k for both footings. The results indicate lesser rotations for higher R_k. The rate of decrease in I_θ reduces with increase in R_k. The values of I_θ are 12 and 20.37 for R_k=1, for rectangular and circular footing respectively.

Table 1 Ranges of Values of Dimensionless Parameters used

Parameter	Range	Remarks
β	0.0025-0.05	Rectangular Footing
	0.005-0.1	Circular Footing
n	0-0.9	Annular Footing
θ	0-0.1	----
R_k	1-30	Linear Analyses
	1-10	Non-Linear Analyses
q^*	0-0.8	----

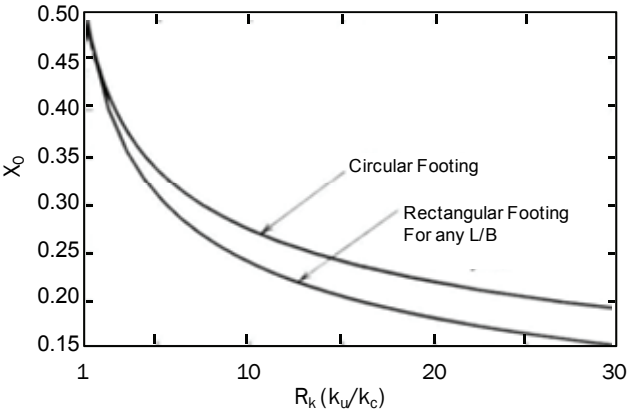

Fig. 51 X_0 verses R_k for Rectangular and Circular Footings – Linear Winkler Model

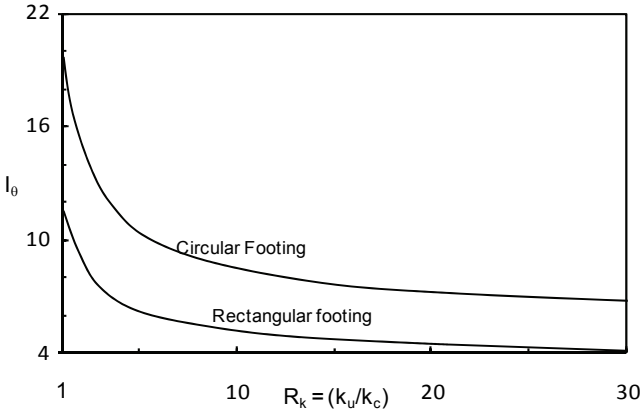

Fig. 52 I_θ verses R_k for Rectangular and Circular Footings – Linear Winkler Model

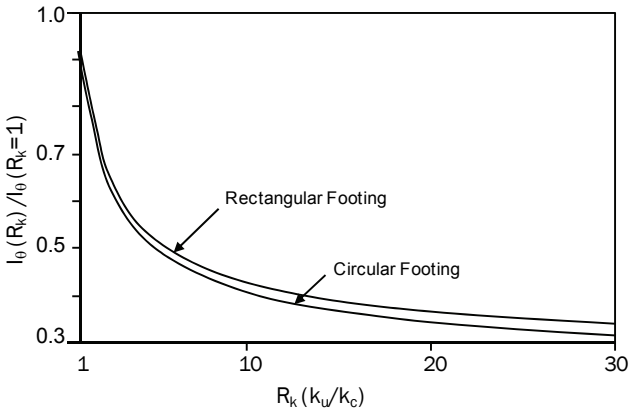

Fig. 53 Normalised I_θ verses R_k for Rectangular and Circular Footings – Linear Winkler Model

These values match exactly with those from Weismann (1972). Figure 53 shows the variation of I_θ normalized with respect to its value at R_k =1 with R_k. The decrease of normalized I_θ with R_k is very high for R_k <2.5 for both types of footings. The rate of decrease in normalized I_θ decreases with increase in R_k. The rate of decrease of normalized I_θ with R_k is nearly the same for circular and rectangular footings. The reduction of I_θ is about 65% of its value at R_k=1 for circular footing and about 63% for rectangular footing for R_k=20.

The effect of R_k on I_θ for annular footings for annular ratio, n, ranging from 0 to 0.9 is shown in Figure 54. Values of I_θ for annular ratio, n, ranging from 0 to 0.3 are nearly the same. I_θ increases with increase in annular ratio due to reduction of the inner solid portion of the annular footing. Figure 55 shows the variation of the ratio of I_θ normalized with respect to its value for R_k=1 with R_k. Normalized I_θ reduces with increase in R_k. Initially the rate of reduction is high but it reduces gradually with further increase in R_k. The rate is almost the same for all annular ratios for R_k <2.5. The rate decreases slightly with increase in annular ratio for R_k>2.5. I_θ reduces to 35% from its value at R_k =1 for a circular footing i.e., annular ratio=0, while for annular ratio of 0.9 the reduction is to about 40% for R_k=20.

The moment - rotation relationships for rectangular footings for different R_k based on nonlinear (hyperbolic response for loading and linear response for unloading) are presented in Figure 56 for β=0.005. The conventional analysis using R_k=1 yields least moment for a given rotation because of least subgrade modulus for unloading. The normalized moment increases for any rotation with increase in R_k. The rate of increase of moment for a given rotation gets reduced with increase in R_k for values beyond 2.

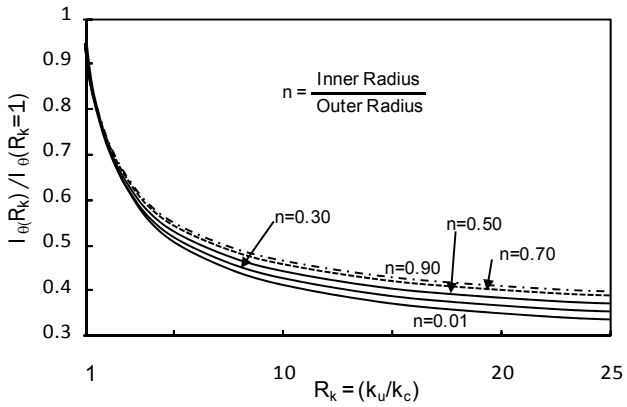

Fig. 55 Normalised I_θ verses R_k for Annular Footings –Linear Winkler Model

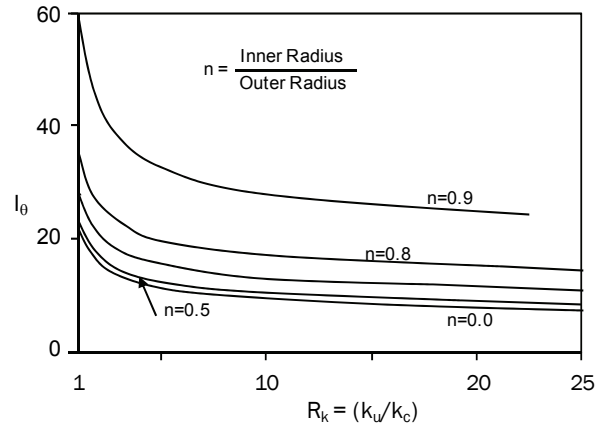

Fig. 54 Effect of R_k on I_θ for Annular Footing Subjected to Moment – Linear Winkler Model

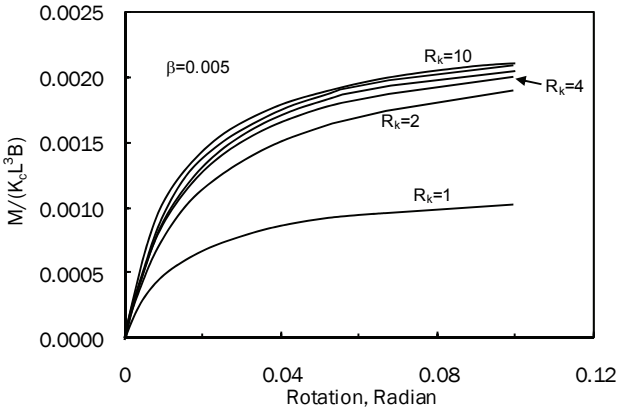

Fig. 56 Effect of R_k on Moment-Rotation Relationship for Rectangular Footing – Nonlinear Winkler Model

Figure 57 shows the effect of β (=q_{ult}/k_cL) on moment-rotation relationship for rectangular footings for R_k=2. β equal to infinity implies linear response and decreasing values of β correspond to lesser values of ultimate stress, q_{ult}. Moment value increases for any rotation with increase in β corresponding to stronger sub-grade. The asymptotic value of moment is reached at much lesser rotation for lower values of β (weaker sub-grade) than that for higher values of β (stronger sub-grade).

The effect of axial load prior to application of moment loading on moment-rotation relationship for rectangular footing based on non-linear model for β=0.005 and R_k=2 is shown in Figure 58. Moment-rotation relationship in case of linear response is not affected by the axial load applied before moment loading. But in case of nonlinear response, axial load softens the soil so that moment loading acts on softened soil. As a result, rotation increases for a particular applied moment as the vertical pressure applied generated prior to the moment application. This pressure is expressed as a fraction of ultimate stress that the soil can undergo and is designated by q^*. Thus the curves become increasingly flatter at higher values of q^*.

The moment-rotation relationship for circular footing for different R_k based on nonlinear analysis for β (=$q_{ult}/(K_cR)$) of 0.01 (Figure 59) is similar to that for rectangular footing. For a particular applied moment, rotation decreases markedly with increase in R_k from 1. The rate of reduction of moment with increasing values of R_k decreases with further increase in R_k. The effect of β on moment-rotation relationship for circular footing based on non-linear analysis for R_k=2 is similar (Figure 60) to that for a rectangular footing (Figure 58). The resisting moment increases for any rotation with increase in β, though the rate of increase with β gets reduced with further increase of β (linear response).

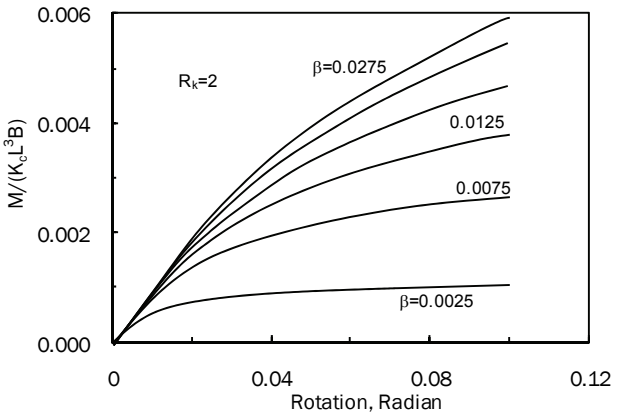

Fig. 57 Effect of β on Moment-Rotation Relationship for Rectangular Footing – Nonlinear Response

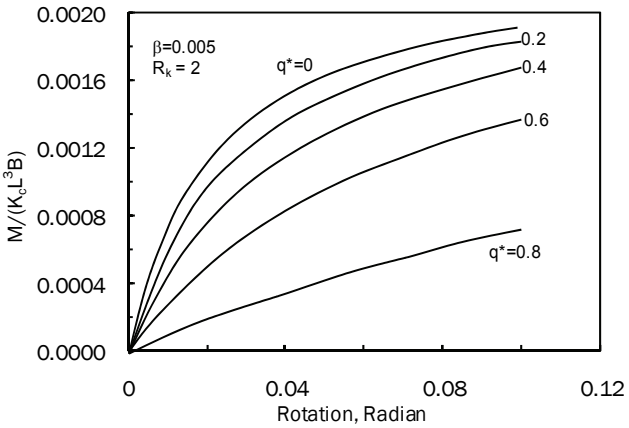

Fig. 58 Effect of Axial Load Prior to Moment Loading on Moment-Rotation Relationship for Rectangular Footing - Nonlinear Response

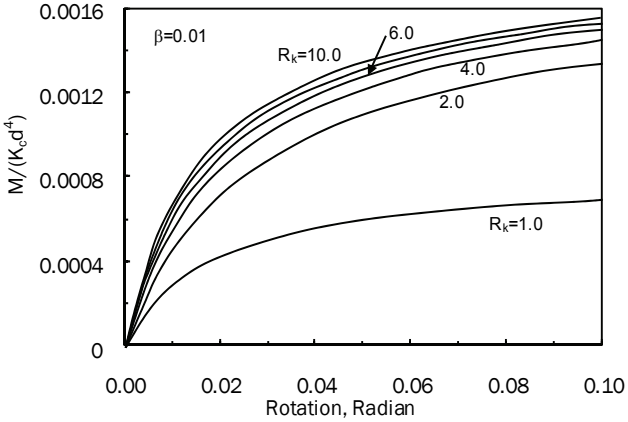

Fig. 59 Effect of R_k on Moment-Rotation Relationship for Rigid Circular Footing - Nonlinear Response

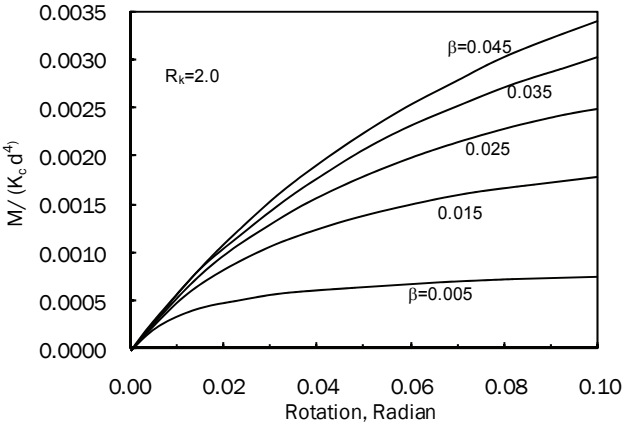

Fig. 60 Effect of β on Moment-Rotation Relationship for Circular Footing – Nonlinear Response

Two Parameter Model with Uncoupled Moduli for Ground

One of the most basic requirements in foundation engineering/soil-foundation interaction problems is the estimation of distribution of displacements and stresses in the soil mass resulting from the loads applied on or near the surface. In practice, loaded areas may be of any shape – circular, square, rectangular, etc. Boussinesq solved the problem of point load acting normal to the surface of an elastic half space. This solution was then integrated for estimating stresses and displacements under shallow foundations of various shapes (footings, rafts, etc.) assuming the soil mass to be an elastic, homogeneous and isotropic half-space.

Hanrahan and Mitchell (1969) and Hanrahan (1971, 1973) proposed a stress, strain and time constitutive model for soils based on the parameters, e_k, (strains chiefly due to change in volume) and e_g (strains chiefly due to change in shape) which are independent of each other unlike in the classical theory of elasticity. Based on the above studies, a simplified two parameter model based on uncoupled deformation (E) and shear (G) moduli, is proposed for estimating stresses and displacements under a rigid or uniformly loaded circular footing. The parameters E and G are measured by conducting the simple direct shear tests, in which soil samples are subjected first to normal and then to shear stresses. The deformation modulus (E) from compression and shear modulus (G) from shear displacement (Noonan and Nixon, 1972) are determined and shown to be independent of each other in most cases.

Foundation – Ground Interaction Models

Winkler proposed a model consisting of a set of unconnected springs to represent the ground assuming the displacement at a point to be directly proportional to the stress applied at that point and independent of stresses and displacements at other points. The two-parameter models (Pasternak, 1954; Filonenko and Borodich, 1945; Hetenyi, 1946; Vlasov, 1949a, b and Reissner, 1958) developed later overcome the discontinuous behavior of Winkler's model. The models developed by Pasternak (1954), Filonenko and Borodich (1945) and Hetenyi (1946) were the extensions of Winkler's model and eliminated the discontinuous behaviour of the model by introducing interaction between Winkler springs through elastic layers, smooth membrane and elastic plate or beam respectively (Selvadurai, 1979). On the other hand, Vlasov (1949) and Reissner (1958) developed models assuming the soil medium as elastic continuum but introducing constraints on displacements and stresses that simplify the basic equations for a linear elastic isotropic continuum (Selvadurai, 1979).

Deformation Parameters E and G

The constrained modulus, D (=$1/m_v$), defined as the inverse of coefficient of volume change, m_v, (Lambe and Whitman, 1970) is obtained from the compression, δ_v, under normal stress, σ, from one dimensional compression test while the shear modulus is obtained from the shear stress – shear displacement relation (Noonan and Nixon, 1972) as $G = T/ k\delta_h$ where T - the shear force, δ_h – the horizontal displacement, and $k = f(\mu, H/L, B/H)$ – a parameter, H and L are respectively the height and length of the sample in simple shear box test and B is the gap between upper and lower halves of the shear box. The values of k are given Figure 61. The moduli of deformation, E_D and E_G could thus be estimated for the two modes of deformation, viz., axial compression and shear deformation respectively as $E_D = D(1+\nu)(1-2\nu/(1-\nu)$ and $E_G = G.2(1+\nu)$ where E_D and E_G are the deformation moduli determined from

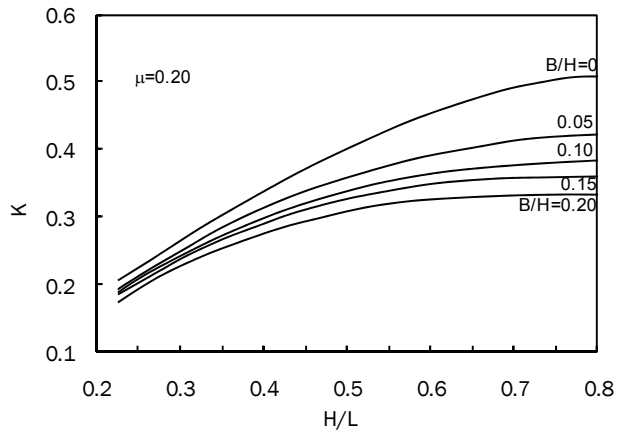

(a)

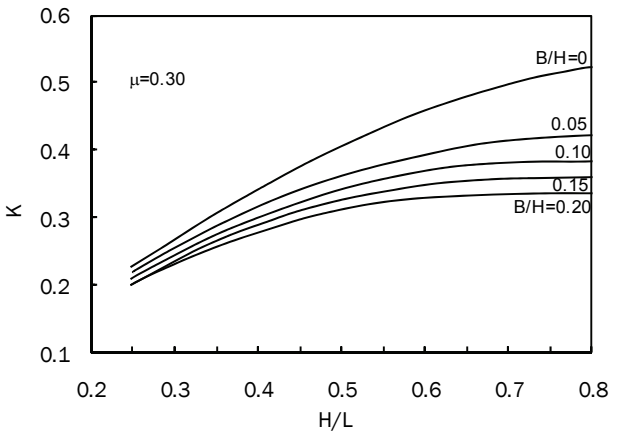

(b)

Fig. 61 Variation of k with H/L for different B/H ratios (a) ν = 0.2 (b) ν = 0.3 after (Noonan and Nixon, 1972)

constrained modulus, D, and shear modulus, G, respectively and ν - the Poisson's ratio of the sample. The parameters E_D and E_G are obtained by conducting direct shear tests on Ganga sand at different relative densities - 35%, 60% and 85% and on clayey silt at different moisture contents - OMC, 2% dry of OMC and 2% wet of OMC. Dimensions of the sample are 6×6×3 cm and the gap 'B' between the shear boxes is close to zero and the normal stress is in the range of 50 to 200 kPa . The analysis is carried out for Poisson's ratio of ν= 0.25. Typical shear stress – horizontal displacement plots for clayey silt at OMC and medium dense Ganga sand at relative density of 60% are given in Figure 62. The variations of moduli computed from shear modulus (E_G) and constrained modulus (E_D) and shear modulus (G) with normal stress are depicted in Figure 63 and the results tabulated in Table 2. The ratio E_G/E_D (Table 2) for sands in dense state is very close to 1 (as predicted by

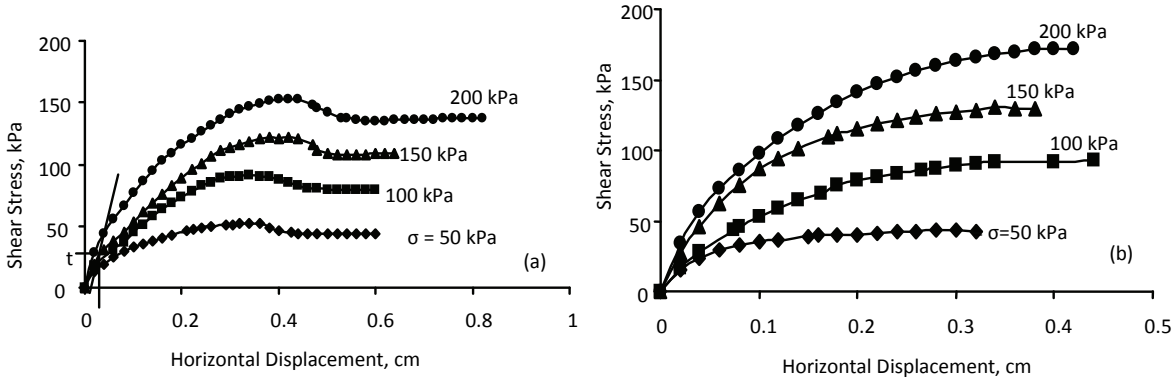

Fig. 62 Typical Results from Direct Shear Tests on (a) Clayey Silt at OMC and γ_{dmax} = 18.4 kPa (b) Medium Dense Sand of Relative Density = 60 %

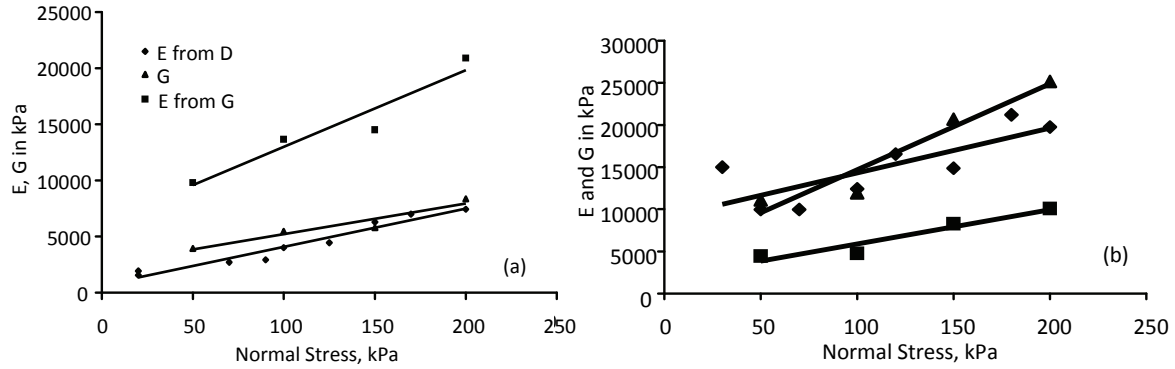

Fig. 63 Typical Results of Variation of Deformation and Shear Moduli with Normal Stress (a) Clayey Silt at OMC and γ_{dmax} = 18.4 kPa (b) Medium Dense Sand of Relative Density = 60 %

Table 2 Moduli from Direct Shear Tests in kPa for Normal Stresses of 50 to 200 kPa

Ganga Sand	Dense State	Medium State	Loose State
G	4700 – 10500	4400 – 10000	1000 – 7000
E_G	11700 – 26200	9500 – 25000	4000 – 11500
E_D	13000 – 25000	11800 – 19200	10000 – 16500
E_G/E_D	0.9 – 1.048	0.80 – 1.30	0.4 – 0.7
Clayey Silt	at OMC (γ_{dmax} = 1.84 g/cc)	2 % Dry of OMC (γ_d = 1.81 g/cc)	2 % Wet of OMC (γ_d = 1.79 g/cc)
G	4000 – 8200	5300 – 10000	2200 – 8200
E_G	9800 – 20000	13000 – 25000	5500 – 20700
E_D	2100 – 7900	3000 – 8400	2400 – 6100
E_G/E_D	4.7 – 2.5	4.3 – 3.0	2.3 – 3.5

classical theory of elasticity) but significantly different from 1 for sands in loose to medium dense state indicating that the parameters E and G are independent of each other. The ratios E_G/E_D are significantly high (2.3 to 4.7) for all moisture contents for clayey silt indicating that the parameters E and G once again are uncoupled.

New Two Parameter Model with Uncoupled Moduli

A simplified 2-parameter continuum model is proposed (Madhav and Raja Sekhar 2010) considering the elastic constants E (deformation modulus) and G (shear modulus) to be independent of each other unlike in the classic theory of elasticity. A uniformly loaded circular footing of diameter 2a, with load of intensity p, (Figure 64a) on the surface of a finite layer of soil mass underlain by a rigid base is considered. Analysis of the problem is available for semi-infinite elastic layer and for finite elastic layer underlain by a rough, rigid base (Burmister 1956; Poulos 1967, Dempsey and Li 1989) based on the elastic continuum approach. In the present study, the soil mass below the footing is assumed as homogeneous and isotropic continuum but characterized by the parameters – deformation modulus, E, and shear modulus, G, independent of each other. As the horizontal displacements, u, are of less engineering interest and are considered to be small for symmetrical vertical loading compared to vertical displacements, w, they are assumed to be zero. The vertical displacements, w, at a radial distance r = 5a are considered to be negligible (Figure 64b). Considering vertical and horizontal force equilibrium of an axi-symmetric element A (Figure 64a), one gets the governing equation in normalized form as,

$$\frac{\partial^2 W}{\partial Z^2} + \mu\left(\frac{\partial^2 W}{\partial R^2} + \frac{1}{R}\frac{\partial W}{\partial R}\right) = 0 \qquad (26)$$

where W = w/a, R = r/a, Z = z/H, and $\mu = (G/E).(H/a)^2$. Eq. (26) is solved numerically for the following cases.

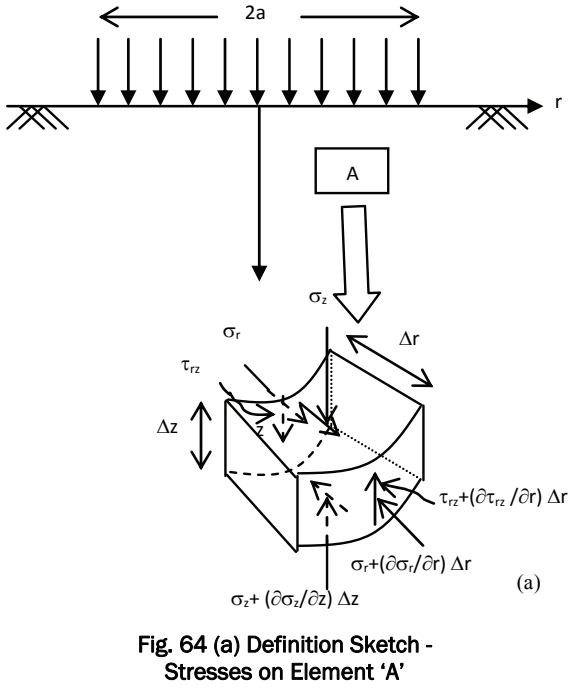

Fig. 64 (a) Definition Sketch - Stresses on Element 'A'

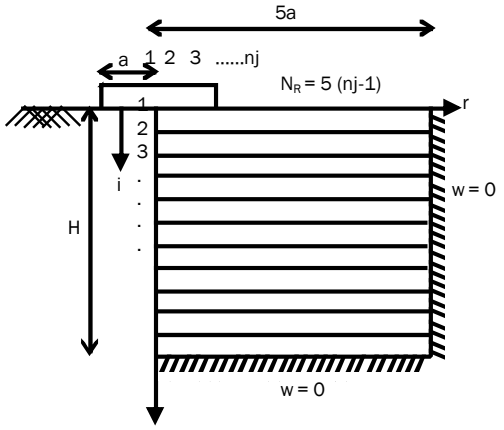

Fig. 64 (b) Definition Sketch Discretisation

Rigid Footing

A uniform displacement, w_o, is imposed at all nodes beneath the rigid footing and the normal stress on the other nodes on the surface are zero. Eqs. (26), are solved iteratively, for the following boundary conditions: $W_{1,j} = W_o$, $W_{n,j} = 0$ and $W_{i,5nj-4} = 0$. Normalizing stress, σ_z, with deformation modulus, E, one gets $\sigma^*_z = -[a/H].\delta W/\delta Z$ where $\sigma_z^* = \frac{\sigma_z}{E}$, $W = \frac{w}{a}$ and $z = \frac{Z}{H}$. Once the displacements are determined, contact pressures beneath the rigid footing are determined.

Uniform Loading

A uniformly loaded perfectly flexible circular footing with load of intensity, p, is considered. The boundary condition is: at z = 0 and for $-a \le r \le a$ is $-E[\delta w/\delta z] = p$

Normalized displacements under the flexible footing are determined by solving Eq. (6) iteratively for a particular value of p^*, as

$$W1,j = \frac{2W_{2,j} + p^*\left(\frac{H}{a}\right)\left(\frac{1}{N_H}\right) + \mu_1\left[\begin{array}{l} W_{1,j-1}\left(1 - \frac{\Delta R}{2R_j}\right) + \\ W_{1,j+1}\left(1 + \frac{\Delta R}{2R_j}\right) \end{array}\right]}{2(1+\mu_1)} \qquad (27)$$

Results and Discussion

Rigid Footing

Displacements: Displacements under the footing, both beneath the center and the edge, decrease with depth rapidly in the top, (z/a) < 3, for G/E = 1 to10 and gradually for G/E = 0.1 to 0.5 (Figure 65). Displacements at all depths decrease with increase in ratio of moduli, G/E. Displacements tend to be almost zero at a normalized depth, z/a, equal to 3 to 4 for deposits of thickness, H/a = 20 for G/E ≥ 5. Boussinesq's curve for displacements beneath the center of the footing lies between the curves for G/E = 0.2 and 0.5 for z/a ≤ 6, are (Figure 65a) more compared to those from the present study for G/E = 0.2 for z/a > 6 and larger than those predicted by the uncoupled theory at all depths for all values of G/E (0.1 to 10) beneath the edge of the footing (Figure 65b). The variation of normalized displacements with normalized depth for deposits of thicknesses, H/a = 1 to 20, are depicted in Figure 66.

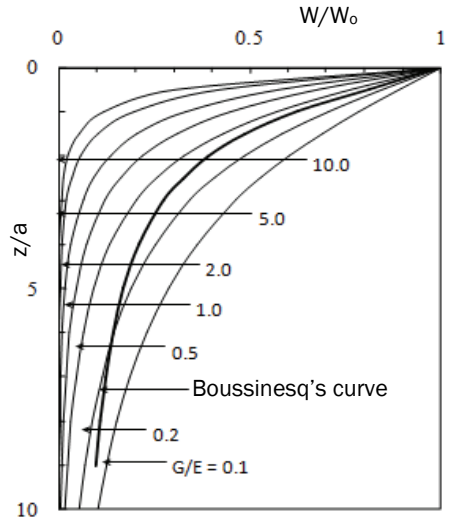

Fig. 65 (a) Normalized Displacements versus Depth Effect of Shear Stiffness at Centre of Rigid Footing

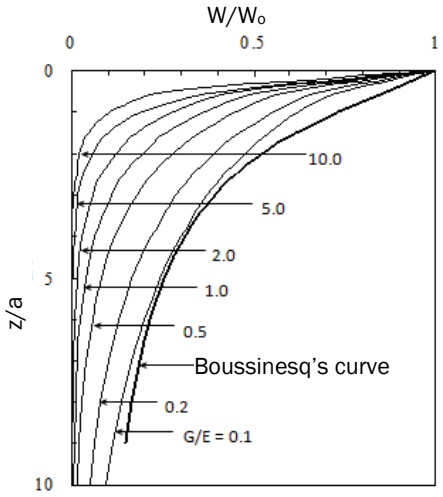

Fig. 65 (b) Normalized Displacements versus Depth Effect of Shear Stiffness at Edge of Rigid Footing

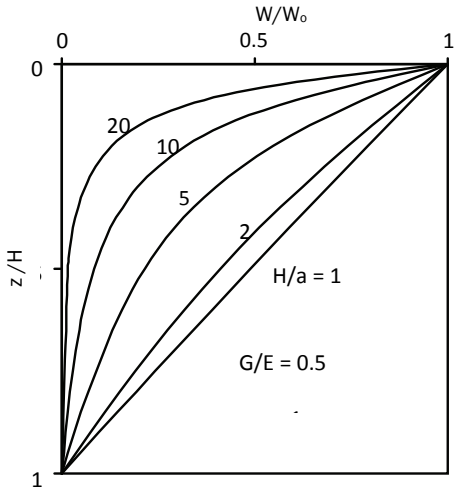

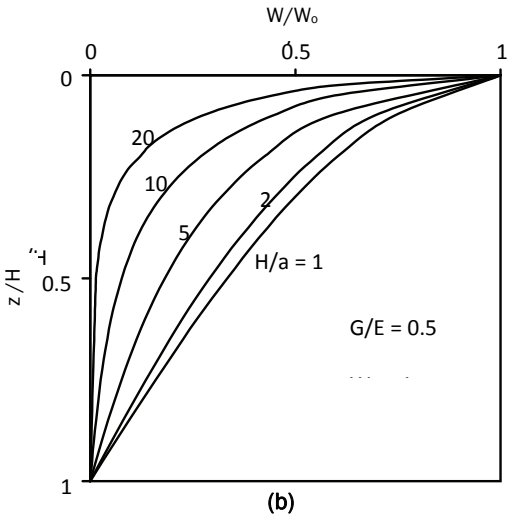

Fig. 66 Normalized Displacements versus Normalized Depth Effect of Layer Thicknesses beneath (a) Center and (b) Edge of Rigid Footing

Contact Pressures: Normalized contact pressures beneath the rigid footing are almost constant up to r/a = 0.8 and 0.5 for soils for G/E = 0.1 and 0.2 & for 0.5 to 10 respectively. Stresses increase sharply for r/a > 0.8 and attain maximum values at the edge of the footing (Figure 67a). The maximum stresses at the edge of the footing increase for G/E increasing up to 0.5 and decrease with further increase in G/E (Figure 67a). The increase is very sharp for soils with G/E = 0.1 and 0.2. The contact pressures at the center decrease with increase in stiffness, G/E, (Figure 67a) and thickness, H/a, (Figure 67b) of the deposit. The contact pressures for deposits with H, > 5a, are almost the same for G/E = 0.5.

Uniform Loading

Displacements: The variations of displacements with depth under the footing with uniform normalized load, p^*, are depicted in Figure 68. Normalized displacements decrease rapidly with depth, z/a, beneath the center and the edge of the footing for soils with G/E = 1 to 10, and gradually for soils with G/E = 0.1 to 0.5. The settlements beneath center of the footing from Boussinesq's solution match well with those for soils with G/E = 0.2 for z/a ≤ 4 (Figure 68a). The displacements from Boussinesq's solution lie between those for soils with G/E = 0.1 and 0.2 for z/a > 4. Displacements beneath the edge, from Boussinesq's

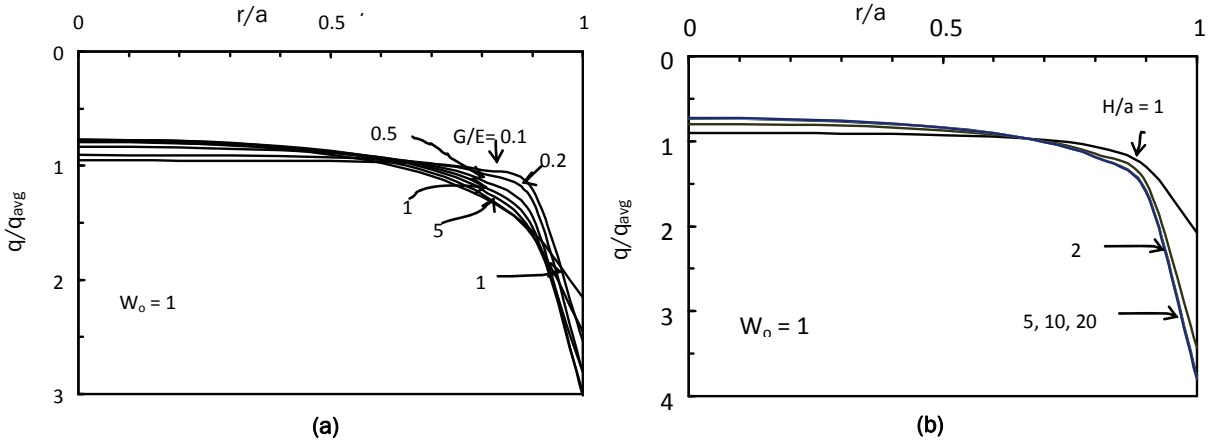

Fig. 67 Distribution of Contact Pressures under the Rigid Footing
(a) for H/a = 1.0 (b) G/E = 0.2

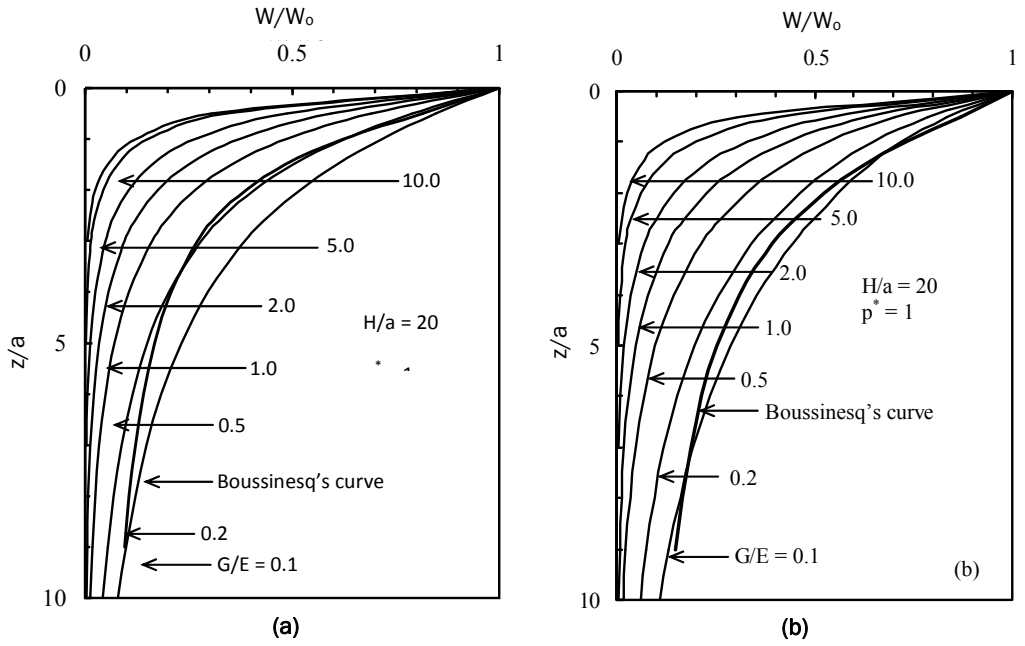

Fig. 68 Normalized Displacements versus Depth – Effect Shear Stiffness of Soil;
Uniform Loading (a) at Center (b) at Edge

solution are slightly more than those for G/E = 0.1, for z/a ≤ 1. The displacements lie between those for soils with G/E = 0.1 and 0.2 for 4 < z/a ≤ 7 (Figure 68b). Boussinesq's solution overestimates the settlements, both beneath the centre and the edge of the footing for stiff soils. The variation of normalized displacements with normalized depth for deposits of thicknesses, H/a = 1 to 20, are depicted in Figure 69.

The vertical surface displacements beneath the footing decrease with increase in stiffness and are nearly constant along the footing for soils with G/E = 0.1 to 10 for r/a ≤ 0.5 (Figure 70a). The displacements decrease gradually for r/a > 0.5. The decrease in displacements is more for soils with G/E = 0.1 to 2 compared to those for soils with G/E = 5 to 10. The vertical surface displacements under uniformly loaded footing resting on the deposits of thicknesses, H > 5a, are almost the same for G/E = 0.5 (Figure 70b).

Vlasov and Leontiev (1966) proposed a two parameter model assuming exponential decrease of displacements with depth. The proposed exponential function is

$$h(z) = \frac{\sinh\eta'(1 - z/H)}{\sinh\eta'} \qquad (28)$$

where $\eta' = \eta H$ - a function of G/E, H/a and r/a. The parameter, η', determines the rate of decrease of displacements with depth (Scott 1981). Jones and Xenophontos (1977) found Eq. (28), proposed by Vlasov and Leontiev (1966), to be fairly accurate for finite layer problems (Scott 1981).

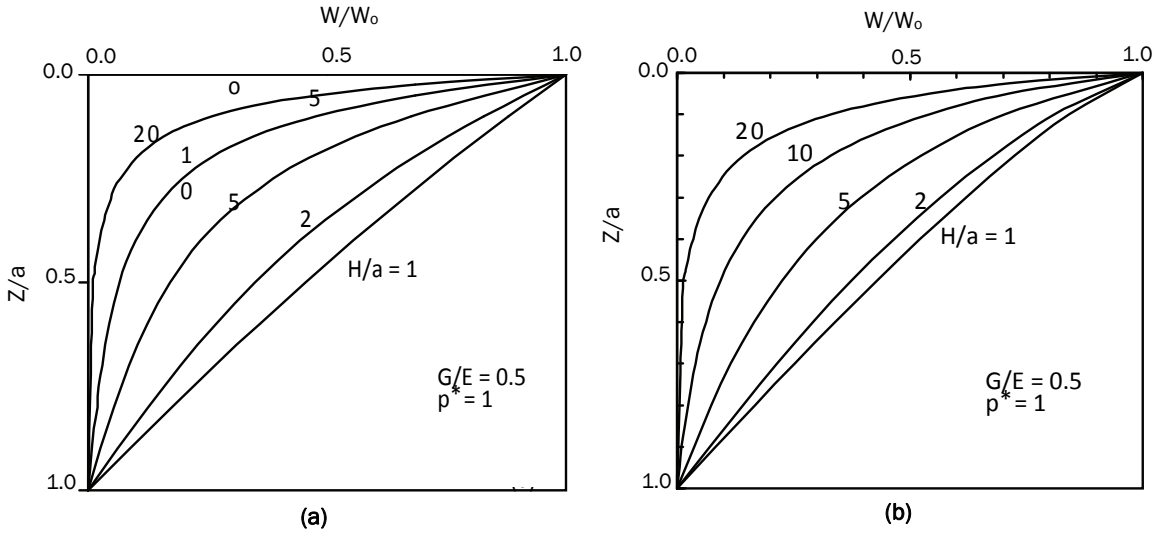

Fig. 69 Normalize Displacements versus Normalized Depth, z/H, - Effect of Thickness; Uniform Loading (a) at Center and (b) at Edge

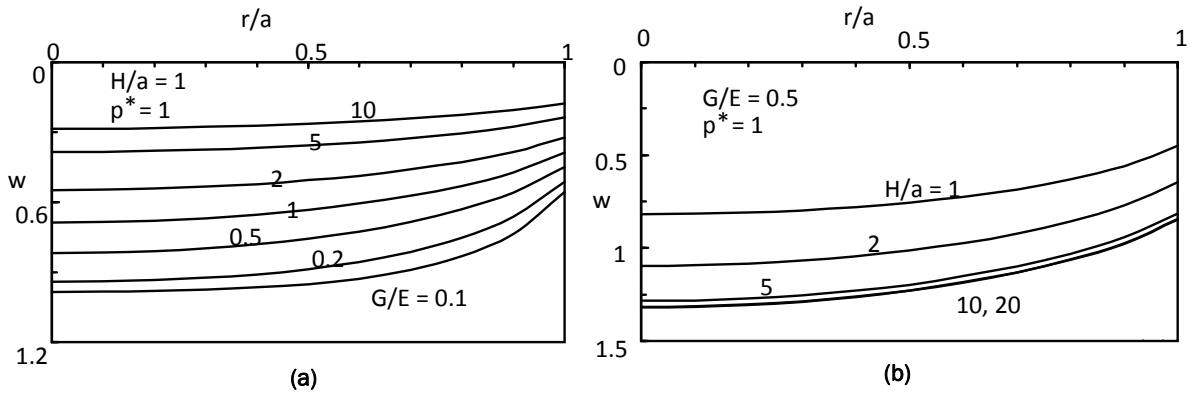

Fig. 70 Distribution of Displacements along the Radius of Footing (a) for H/a = 1 (b) for G/E = 0.5

The variation of η' with G/E (Figure 71), for both flexible and rigid circular footings, is estimated for soil layers of different thickness, H/a. The variation of vertical displacements with depth proposed by Vlasov and Leontiev (1966), are determined for uniformly loaded circular footing for G/E = 1.0, H/a = 2.0 and η' = 2.3 for settlements beneath the center and the edge. Similarly, the variations of displacements with depth under the rigid circular footing are determined for G/E = 0.5, H/a = 2.0 and η' = 1.26 beneath the center and the edge. The variations of displacements with depth, under the rigid and flexible circular footings, obtained from the proposed new uncoupled model compare well (Figure 72) with those obtained from Vlasov and Leontiev (1966).

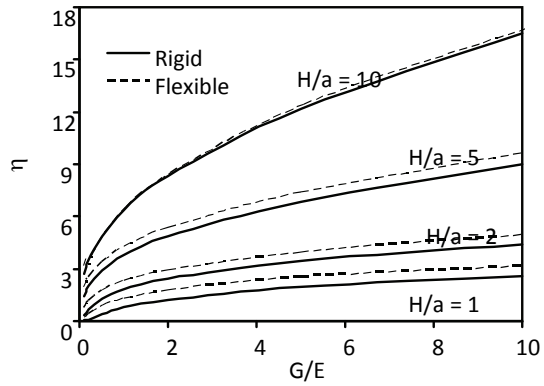

Fig. 71 Variation of Parameter η′ with Relative Stiffness, G/E, - Effect of Thickness, H/a

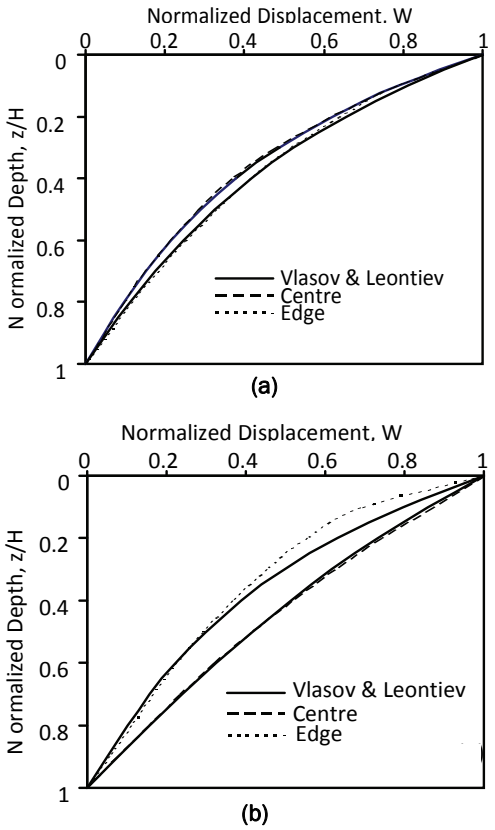

Fig. 72 Comparison of Vertical Displacements with Depth from Proposed 2-Parameter Model under Circular Footing with those from Vlasov and Leontiev (1966) (a) Uniform Loading (b) Rigid Footing

Strain Induced Non-homogeneity of Soils

Stresses and deformations due to applied loads are estimated based on linear elastic and homogeneous conditions. The underlying assumption is that at working loads the soil mass is linearly elastic and that the stress/strain changes in the soil are close to those given by linear elasticity even though the soil response may be nonlinear. Boussinesq solution for the distribution of stresses in a half-space resulting from surface loads is based on the assumption of linear elastic homogeneous isotropic half-space for the soil media. While some writers reported acceptable agreement between experimental results and those from elastic theory (Siddharthan et al. 1996), others observed significant differences which in some cases exceed 200% (Ullidtz et al. 1996). The disparity between the experimental results and the elastic theory could be attributed to nonlinear soil behavior, anisotropy, stress or strain induced non-homogeneity, etc. Schmertmann's method (Schmertmann et al., 1978) is ideally suited to estimate the settlement of footings for the cases with material non-homogeneity (i.e., the deformation modulus of the soil, E_s, varies with depth as measured through e.g., CPT) based on the assumed variation of strain influence factor with depth.

A typical plot (Figure 73, next page) of variation of secant modulus with deviatoric strain (Fahey and Carter 1993) illustrates the strong decrease of the modulus even in pre-failure deformation or strain range. The variation of modulus of deformation, E, with strain, ε, can be expressed in the form,

$$E = E_{max}/\{1 + (\varepsilon/\alpha)^{\beta}\} \qquad (29)$$

where E_{max} is the small strain modulus and α and β are parameters.

Analysis

A circular footing, 4.0 m in dia. resting on the surface of cohesionless soil with angle of shearing resistance of 32°, deformation modulus of 20 MPa and Poisson's ratio: 0.3, subjected to a uniform nominal load of 10 kPa is analyzed using PLAXIS. Radial deformation

is restricted but vertical deformation is allowed along the lateral boundaries. Both radial and vertical deformations are restricted along the bottom surface. An iterative technique is developed starting with homogeneous condition, i.e., modulus is independent of location. Strain contours are obtained from the primary iteration and corresponding deformation moduli estimated using Eq. 29. Each subsequent analysis uses the evaluated moduli at average points that correspond to the strain level within that zone. The problem of uniform circular load on the surface is reanalyzed with the new set of deformation moduli. The procedure is repeated till convergence is achieved for stresses, displacements, strains and deformation moduli.

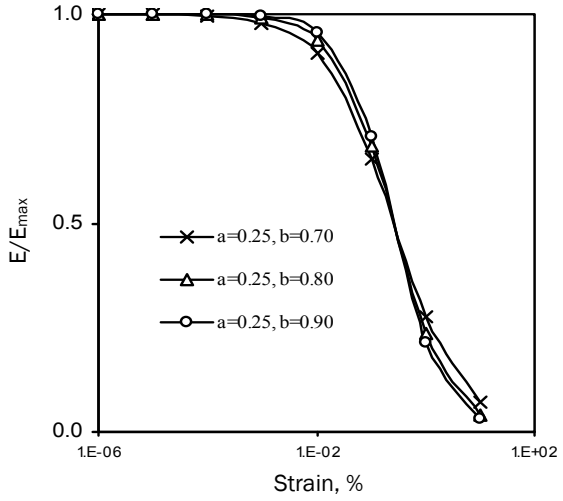

Fig. 73 Normalised Deformation Modulus vs Strain (after Fahay and Carter 1993)

Results and Discussion

The final strain contours for a typical case of H/D = 1.0 is presented in Figure 74. The variations of vertical strain with depth are presented in Figure 75. The vertical strain increases up to a certain depth and reduces for depths greater than the above value for all depth to diameter ratios of 0.5, 1.0, 2.0 and 4.0 as suggested by Schmertmann (1970). The depth at which the strain attains the maximum value reduces with increasing depth ratios. The depth to maximum strain is 0.5H for H/D of 0.50 and 0.1H for H/D of 4.0. The variations of final or converged deformation moduli with depth for H/D of 0.50, 1.0, 2.0 and 4.0 are presented in Figure 76. It should be noted that the medium is homogenous initially with the deformation modulus equal to 20 MPa everywhere. The deformation modulus decreases with depth near the top close to the surface to attain a minimum value and increases thereafter to all depth to diameter ratios. The modulus of deformation is of the order of 16 to 17 MPa for a thin layer of H/D =

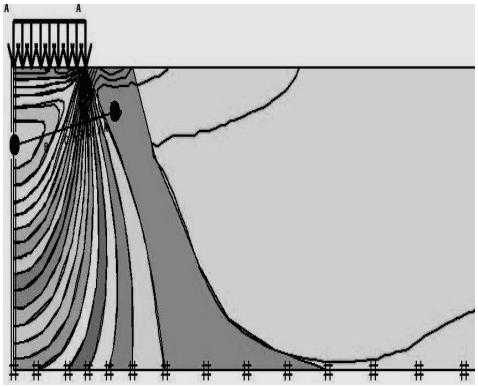

Fig. 74 Vertical Strain Contours for H/D = 1.0

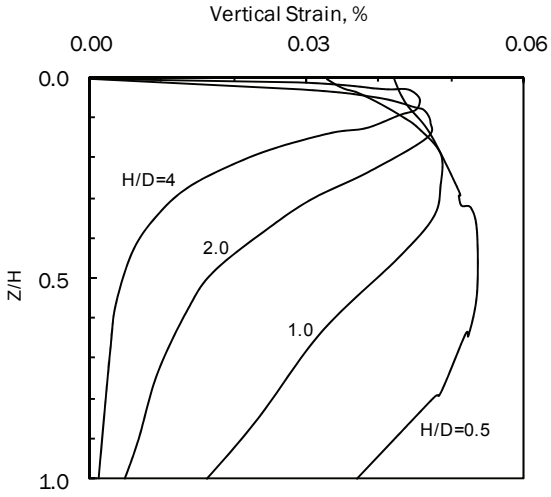

Fig. 75 Variation of Strain with Depth

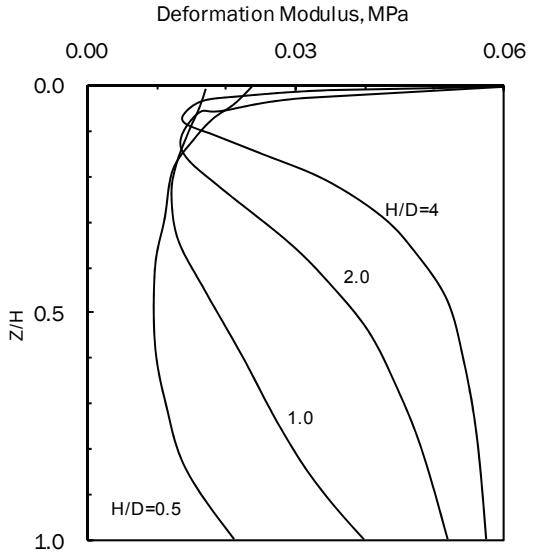

Fig. 76 Variation of Final Deformation Moduli with Depth

0.50. For larger thickness of the ground, the modulus of deformation increases with depth from the minimum value and in case of a very thick deposit attains the initial value of 20 MPa where the strains are negligibly small. Thus non-homogeneity is induced in the medium because of strain attained at that particular point.

Conclusions

Geotechnical Engineers are highly indebted to Karl Terzaghi for founding the discipline in mid 1920s. The subject has grown by leaps and bounds due to the efforts succeeding academics and practitioners. SM & GE is celebrating the Platinum Jubilee in November 2010. It is an appropriate time to review some of the basic tenets introduced by Terzaghi nearly eighty years ago. We now have a much better understanding of the complexity of soil as an engineering material and ground as an entity. This paper examines some of those basic assumptions, viz., rigid plasticity and non-consideration of the structure in estimating bearing capacity of foundations, the extension of theory of consolidation for thin layers based on linear void ratio – effective stress relation to thicker deposits and soils that follow linear void ratio – log effective stress relation, inelasticy of ground and its effect on moment – rotation relationships, uncoupling deformation and shear moduli based on experimental evidence and its incorporation in a simple foundation model, etc., made in the early formative years.

Conventional approaches for the estimation of the ultimate capacities of both shallow and deep foundations use limit equilibrium methods and are based on only the strength parameters apart from the geometry of the foundation element. Ground/soil being a much more complex material than metals from which the original theories have been developed, requires the consideration of stiffness or compressibility as well as the strength parameters for the estimation of ultimate loads. The results for the bearing capacity of shallow

foundations and the ultimate axial capacity of piles illustrate their dependence on the stiffness of the ground. Consideration of height of a structure rather than just only the foundation leads a very interesting and unique failure state, the leaning instability of tall structures that is governed by the stiffness of the ground rather than the strength.

A simple and approximate non-linear theory of one-dimensional consolidation for thick clay layer is developed. The conventional thin layer theory under-estimates the degree of consolidation but over-estimates the degree of dissipation of excess pore pressures. The isochrones in the case of a thick layer with PTPB condition are slightly unsymmetrical about the mid depth in contrast to symmetrical isochrones in thin layer theory. The degree of settlement and degree of dissipation of pore pressures are sensitive to the magnitude of loading in the case of a thick layer while these are independent of loading in the thin layer theory.

One of the major findings of the non–linear theory of consolidation for both vertical and radial flows is that while the degree of settlement is independent of the final to initial stress ratio, the degree of dissipation of pore pressure is very much dependent on the stress ratio. The residual excess pore pressures are underestimated in the conventional linear theory. The present theory substantiates the actual in-situ slower rate of degree of dissipation of excess pore pressures compared to that of the degree of settlement. The degree of dissipation of excess pore pressure decreases with increase of the stress ratio. This ratio varies with depth, and is relatively large at shallow depths where initial stress is very less. Hence the non-linear consolidation effect is pronounced at shallow depths compared to the effect at greater depths. A major finding of the present work is that the excess pore pressures due to radial drainage vary not only with time and radial distance but also with depth in contrast to depth-independent pore pressures from the conventional theory for radial flow. That is, while pure radial flow consolidation may be valid for thin layers, no such assumption can be made for thicker layers. The effect of non-linear consolidation is more pronounced during the intermediate stages of consolidation. The practical significance of the proposed theory is that it can explain failure of high embankments constructed rapidly on thick deposits of fine grained soils as the stress ratio at shallow depths would be significantly high leading to slower rate of dissipation of pore pressures and higher residual pore pressures.

The inelastic response of the ground needs to be considered for the analysis of rigid foundations subjected to moment loading. The inelastic response is characterized by the stiffness ratio, R_k, defined as the ratio of subgrade moduli in unloading to that in compression. The ratio, R_k, and the non-linear stress – displacement response have very significant effect on the overall response of footing to applied moment loading. The axis of rotation shifts towards the unloading side from the center of the contact area with increase of R_k. The rate at which the axis of rotation gets shifted reduces gradually with increase of R_k. The moment influence coefficient, I_θ decreases with increase in R_k implying that the conventional approach over-estimates the rotation of footings due to moment loading. The rate of decrease of I_θ with R_k reduces gradually. The normalized values of I_θ for any R_k with respect to the corresponding value at R_k=1 are nearly the same for rectangular and circular foundations. I_θ for annular footings for any R_k varies marginally with increase in annular ration for n < 0.5 but increases markedly for n > 0.5. The variation (decrease) of normalized I_θ with R_k is almost independent of annular ratio, n. Results based

on nonlinear response of the ground are similar to the response based on linear models. The rotation of footing caused by a moment loading on a nonlinear model is more if an axial load is acting prior to the application of moment loading.

A new two parameter continuum model with uncoupled moduli is proposed to estimate the vertical displacements and contact pressures under rigid and flexible circular footings. The proposed uncoupled model is validated by comparing the variations of displacements with depth with those from Vlasov and Leontiev (1966). It is observed that in case of rigid footing, the Boussinesq's curve at centre of the footing falls between G/E = 0.2 and 0.5 and at edge the displacements are more near the top than those obtained from 2-parameter model for all G/E values. In case of flexible footing, the displacements from Boussinesq's solution at centre of the footing matches closely with those for G/E = 0.2 till z/a = 4 and thereafter the Boussinesq's curve falls between G/E = 0.1 and 0.2. The Boussinesq's curve almost matches closely with G/E = 0.1 at the edge till z/a =1.5 and thereafter falls between G/E = 0.1 and 0.2. Boussinesq's solution over predicts the vertical displacements in case of stiff soils (G/E = 5 to 10) under rigid and flexible footings.

The contact pressures beneath the rigid footing increase very sharply near the edge of the footing for soils with G/E = 0.1 to 0.5 and are same for soil layers, with same stiffness, G/E = 0.2, of thickness greater that 5 a. The vertical surface displacements beneath the flexible footing decrease with increase in stiffness of soil and are almost constant along the footing for stiff soils (G/E = 5 to 10). But for soils with G/E = 0.1 to 2 the vertical surface displacements decrease along the footing and the rate of decrease is more near the edge. The vertical surface displacements beneath the flexible footing increase with increase in thickness of the soil layer but are almost the same for layers of thickness, H, greater than 10.a.

The stresses and strains in soil mass depend on the stress-deformation characteristics, anisotropy and non-homogeneity of the medium. Recent research has established the variation of deformation modulus with strain level. The problem of deformation response of a uniformly loaded circular footing on an initially homogeneous medium of finite thickness is analyzed incorporating the variation of deformation modulus with strain. The medium becomes non-homogeneous because of strain induced non-homogeneity. The degree of non-homogeneity depends on the relative thickness of the deposit.

Acknowledgments

This work would not have day-lighted without the contributions of a large number of former and current graduate students, Saha, Rajasekhar, Manoj, Padmavathi, Ayub Khan, Lakshmana Rao, Suresh, Vidyaranya, etc., who have worked hard over several years to concretise the ideas enunciated in this paper. I am always indebted to my students who have made me. The contribution of Dr Umashankar in formatting the paper is gratefully appreciated.

References

Almeida, M.S.S., Santa Maria, P.E.L., Martins, I.S.M., Spotti, A.P. and Coelho, L.B.M. (2000): 'Consolidation of very soft clay with vertical drains', *Geotechnique,* 50(6), 633–643.

Ayub Khan, P., Madhav, M.R. and Saibaba Reddy, E. (2009): 'Non-linear Theory of Consolidation of Thick Layer Clay Layer by PVD. *Int. Symp. on Ground Improvement Technologies and Case Histories*', Singapore, 337-344.

Ayub Khan, P., Madhav, M.R. and Saibaba Reddy, E. (2010): 'Simplified Non-Linear Theory of Vertical Consolidation of Thick Clay Layers', *IGC 2010*, Mumbai.

Barron, R.A. (*1948*): 'Consolidation of fine grained soils by drain wells', *Trans. ASCE*, 113, 718–754.

Basak, P. and Madhav, M.R. (1978): 'Analytical solution of sand drain problems', *J of Geotech. Engrg, ASCE*, 104(1), 129–135.

Bergado, D.T., Balasubramaniam, A.S., Fannin, R.J. and Holtz, R.D. (2002): 'Prefabricated vertical drains (PVDs) in soft Bangkok clay: a case study of the new Bangkok International Airport project', *Can.Geotech, J.*, 39, 304-315.

Borowicka, H. (1943): ‚Uber ausmittig belaste starre platen auf elastic-isotropem Unter grund'. *Ingenier-Archiv,* Berlin, 1, 1-8.

Burmister, D.M. (1956): 'Stress and Displacement Characteristics in Two-Layer Rigid Base soil System: Influence Diagrams and Practical Applications'. P*roc. HRB*, 35, 773.

Cheney J.A., Abghari A. and Kutter B.L. (1991): 'Stability of Leaning Towers'. *J Geotech. Eng.*, Proc. ASCE, 117(2), 297-318.

Conte, E. and Troncone, A. (2009): 'Radial consolidation with vertical drains and general time-dependent loading', *Can. Geotech. J.*, 46, 25-36.

Davis, E.H. and Raymond, G.P. (1965): A nonlinear theory of consolidation, *Geotechnique*, 15(2), 161–173.

Dempsey, J.P. and Li, H. (1989): 'A Rigid Rectangular Footing on an Elastic Layer', *Geotechnique*, 39, 147-152.

Egorov, K.E., Barvashobv, V.A. and Fedorovsky, V.G. (1973): Some Application of Elasticity Theory to Design of Foundations. *Proc. 6th Int. Conf. SMFE*, Moscow, 1(3), 60-74.

Egorov, K.E., Kitaikina, O.V. and Zinovyev, A.V. (1979): Deformation of Ring Foundation Base. *Proc. 6th Asian Regional Conf. SMFE*, Singapore, 1, 281-284.

Egorov, K.E., Vronsky, A.V., Finseva, T.V. and Illynykh, V.A. (1980): Study of the Stress and Strain State of a Subgrade under an Eccentric Load. *Proc. 8th Danube-European Conf.SMFE*, Varna, Bulgeria, 2, 67-78.

Egorov, K.E. and Vronsky, A.V.(1980): Study of Stress and Strain Rate of a Subgrade under an Eccentric Load. *Proc. 8th Danube-European Conf. SMEF*, Varna, 2, 67-78.

Fahey M and Carter J.P. (1993): "A finite element study of the pressuremeter in sand using a nonlinear elastic plastic model" *Canadian Geotechnical J.* 3, 348-362.

Filonenko-Borodich, M. M. (1945): *A Very Simple Model of an Elastic Foundation capable of Spreading the Load*. Sb. Tr. Mosk. Elektro. Inst. Inzh. Trans. No: 53 Transzheldorizdat (in Russian).

Gazetas, G. (1998): 'Elastic Formulae for Lateral Displacement and Rotation of Arbitrarily-shaped Embedded Foundations'. *Geotechnique*, 38(3), 439-444.

Georgiadis, M. and Butterfield, M. (1988): 'Displacements of Footings on Sand under Eccentric and Inclined Loads'. *Canadian Geotech. J.*, 25, 199-211.

Gibson, R. E. and Anderson, W. F. (1961): 'In-situ measurements of soil properties with the pressuremeter'. *Civ. Engng Public Wks. Rev.*, 56, 615-618.

Gibson, R.E., Schiffman, R.L. and Cargill, K.W. (1981): 'The theory of one-dimensional consolidation of saturated clays: II. Finite nonlinear consolidation of thick homogeneous layers'. *Can. Geotech J,* 18(2)280-293.

Hambly, E.C. (1985): 'Soil Buckling and Leaning Instability of Tall Structures'. *Structural Engr*. 63A(3), 77-85.

H Hambly, E.C. (1990): 'Overturning Instability'. *J. of Geotechnical Engineering*, ASCE, 116(4), 704-709.

Hanrahan, E.T and Mitchell, J.A. (1969): 'The Importance of Shear in Consolidation.' *Proc. of 7th ICSMFE*, Mexico, 1, 183-190.

Hanrahan, E.T. (1973): 'The Stress-Strain Relationship in Soil Mechanics." *Trans*., Inst. of Engrs of Ireland, 97.

Hanrahan, E.T. (1971): 'The e_g and e_k Parameters'. *Roscoe Symp*., Cambridge, 362-367.

Hansbo, S. (1979): 'Consolidation of clay by band shaped prefabricated drains', *Gr. Engg*, 12(5)16-25.

Hansbo, S. (1981): 'Consolidation of fine grained soils by prefabricated drains', *Proceedings of the 10thICSM&GE,* Stockholm, Sweden, 3, 667-682.

Hetenyi, M. (1946): *Beams on Elastic Foundations*. University of Michigan Press, Ann Arbor, Michigan.

Jones, R and Xenophontos, J. (1977): 'The Vlasov Foundation Model'. *Int. Journal of Mech. Sc*., 19, 317-323.

Indraratna, B., Bamunawita, C., Redana, I.W and McIntosh, G. (2003): Modeling of prefabricated vertical drains in soft clay and evaluation of their effectiveness in practice, *Gr. Impr.*, 7(3), 127–137.

Indraratna, B., Rujikiatkamjorn, C. and Sathananthan, I. (2005a): 'Radial consolidation of clay using compressibility indices and varying horizontal permeability,' *Can. Geotech. J.*, 42(5), 1330–1341.

Indraratna, B., Sathananthan, I., Rujikiatkamjorn, C. and Balasubramaniam, A.S. (2005b): 'Analytical and numerical modeling of soft soil stabilized by prefabricated vertical drains incorporating vacuum preloading', *I J of Geomechanics,* 5(2)114–124.

Indraratna, B., Rujikiatkamjorn, C. and Chu, J. (2007): 'Soft clay stabilization with geosynthetic vertical drains beneath road and railway embankments: A critical review of analytical solutions and numerical analysis', *Advances in Measurement and* Modeling *of Soil Behavior (GSP173),* 236, 7.

Indraratna, B., Aljorany, A. and Rujikiatkamjorn, C. (2008): 'Analytical and numerical modeling of consolidation by vertical drain beneath a circular embankment', *I J of Geomech.,* 8(3), 119–206.

Lambe, T.W and Whitman, R.V. (1969): *Soil Mechanics*, John Wiley & Sons, New York, 151-161.

Lancelotta, R. (1993): 'Stability of a Rigid Column with Non-linear Restraint'. *Geotechnique*, 43(2), 331-332.

Lekha, K.R., Krishnaswamy, N.R. and Basak, P. (1998): 'Consolidation of clay by sand drain under time–dependent loading', *J of Geotechnical* and *Geoenvironmental Engineering*, 124(1), 91-94.

Madhav, M.R. and Miura, N. (2004): 'Phase transition effect on preconsolidation stress of soil', *Indian Geotechnical Journal*, 34(1), 80-95.

Madhav, M.R. and Padmavathi, V. (2008): 'Effect of Stiffness of Ground on Ultimate Capacity of Foundations', *Proc. IGC 2008*, Bangalore.

Madhav, M.R., Padmavathi, V., and Saha, S. (2009): 'Inelastic Response and Moment – Rotation Relationship of Foundations', *IGC 2009*, Guntur.

Madhav, M.R. and Raja Sekhar, M. (2010): 'New Two Parameter Model with Uncoupled Moduli for Ground', *IGC 2010,* Mumbai.

Menard, L. (1957d): 'Mesures in situ des propriétés physiques des sol's', *Annales des Ponts et Chaussées*, Paris, 14, 357-377.

Noonan, D.K.J and Nixon, J.F. (1972): 'The Determination of Young's Modulus from the Direct Shear Test'. *Canadian Geotechnical Journal*, 9, 504-507.

Pasternak, P.L. (1954): 'On a New Method of Analysis of an Elastic Foundation by means of Two Foundation Constants'. *Gosudarstvennoe Izdatelstro Liberaturipo Stroitelstvui Arkhitekture*, Moscow (in Russian).

Potts, D. M. (2003): 'Numerical Analysis: A Virtual Dream or Practical Reality'. *Rankine Lecture, Geotechnique*, 53(6) 535-572.

Poulos, H.G. and Davis, E.H. (1974): E*lastic Solution for Soil and Rock Mechanics*. John Wiley & Sons, NY, 43-54.

Poulos, H.G. (1967): 'Stresses and Displacements in an Elastics Layer Underlain by a Rough Rigid Base'. *Geotechnique*, 17, 378-410.

Reissner, E. (1958): 'Deflection of Plates on Viscoelastic Foundation'. *J Appd Mech*., 80, 144-145.

Richart, F.E. (1959): 'Review of the theories for sand drains', *Trans. of ASCE*, 124(2999), 709–736.

Rujikiatkamjorn, C. and Indraratna, B. (2006): 'Three-dimensional numerical modeling of soft soil consolidation improved by prefabricated vertical drains', *Ground Modification and Seismic Mitigation (GSP 152),* 196, 22*,* 161–168.

Rujikiatkamjorn, C., Indraratna, B. and Chu, J. (2008): '2D and 3D numerical modeling of combined surcharge and vacuum preloading with vertical drains', *I J of Geomechanics,* 8(2), 114–156.

Sathananthan, I. and Indraratna, B. (2006): 'Plane-strain lateral consolidation with non-Darcian flow', *Can.Geotech*, *J*.**,** 43, 119-133.

Scott, R.F. (1981): *Foundation Analysis*. Prentice Hall, NJ, 85-118.

Schmertmann, J. H. and Hartman, J.P. (1978): 'Improved Strain Influence Factor Diagrams,' J. of Geotechnical Engrg. Div., ASCE, 104(GT8), 113-1135.

Selvadurai, A.P.S (1979): 'Elastic Analysis of Soil-Structure Interaction', *Developments in Geotechnical Engineering Vol 17*, Elsevier Scientific Publishing Company.

Siddharthan, R.V., Yao, J., and Sebaaly, P. (1996): *Field Verification of a Moving Load Model for Pavement Response*. TRB, National Research Council, Washington, D.C.

Teh, C.I. and Nie, X. (2002): 'Coupled consolidation theory with non-Darcian flow', *Computers and Geotechnics*, 29(3), 169-209.

Terzaghi, K. (1943): *Theoretical Soil Mechanics*. John Wiley & Sons, New York, p. 510.

Terzaghi, K. and Peck, R.B. (1967): *Soil Mechanics in Engineering Practice*. Wiley, New York.

Ullidtz, P., Askegaard, V., and Sjolin, F.O. (1996): *Normal stresses in a granular material under FWD loading*. TRB, National Research Counsil, Washington, D.C.

Vaid, Y.P. (1985): 'Constant rate of loading nonlinear consolidation', *Soils and Foundations*, 25(1), 105–108.

Vesic, A. S. (1972): 'Expansion of Cavities in infinite soil mass'. *J. Soil Mech. And Found. Div.*, ASCE, 98(3), 265-290.

Vesic, A.S. (1973): 'Analysis of Ultimate Loads on Shallow Foundations'. *J. Soil Mech. And Found. Div.*, ASCE, 99(1), 45-73.

Vesic, A.S. (1977): 'Design of Pile Foundations', *National Cooperative Highway Research Program, Synthesis of Practice*, No. 42, Transportation Research Board, Washington, DC.

Vlasov, V.Z. (1949a): 'Structural Mechanics of Thin-Walled Three-Dimensional Systems'. *Gosstroiizdat,* Moscow, Leningard (in Russian).

Vlasov, V.Z. (1949b): 'General Theory of Shells and its Application in Engineering'. G*osterkhizdat*, Moscow, Leningard (in Russian).

Vlasov, V.Z and Leontiev, U.N. (1966): 'Beams, Plates and Shells on Elastic Foundations', I*srael Program for Scientific Translations*, Jerusalem (Translated from Russian).

Walker, R., Indraratna, B. and Sivakugan, N. (2009): 'Vertical and radial consolidation analysis of multilayered soil using the spectral method', *J. Geotech. Geoenv. Eng., ASCE,* 135(5), 657– 663.

Xie, K.H. and Leo, C.J. (2004): 'Analytical solutions of one-dimensional large strain consolidation of saturated and homogeneous clays'. *Computers and Geotechnics*, 31, 301-314.

Xie, K.H., Xie, X.Y. and Jiang, W. (2002): 'A study on one-dimensional nonlinear consolidation of double-layered soil'. *Computers* and *Geotechnics*, 29, 151-168.

Zhuang, Y.C., Xie, K.H. and Li, X.B. (2005): 'Nonlinear analysis of consolidation with variable compressibility and permeability', *J. of Zhejiang University (Engineering Science)*, 6A(3), 181–187